

**SURFACE CHEMISTRY DEPENDENCE
ON MICRORHEOLOGICAL MEASUREMENTS**

by

Becky E. Gable

A thesis submitted to the Faculty of the University of Delaware in partial fulfillment of the requirements for the degree of Bachelor of Chemical Engineering with Distinction.

Spring 2006

Copyright 2006 Becky E. Gable
All Rights Reserved

**SURFACE CHEMISTRY DEPENDENCE
ON MICRORHEOLOGICAL MEASUREMENTS**

by

Becky E. Gable

Approved: _____
Eric M. Furst, Ph.D.
Professor in charge of thesis on behalf of the Advisory Committee

Approved: _____
Christopher J. Roberts, Ph.D.
Committee member from the Department of Chemical Engineering

Approved: _____
Michael Keefe, Ph.D.
Committee member from the Board of Senior Thesis Readers

Approved: _____
Mohsen Badiy, Ph.D.
Chair of the University Committee on Student and Faculty Honors

TABLE OF CONTENTS

LIST OF TABLES	v
LIST OF FIGURES	vi
ABSTRACT	viii
Chapter	
1 MOTIVATION	1
2 INTRODUCTION	3
2.1 Peptide Structure and Chemistry	3
2.1.1 MAX1	3
2.1.2 HPL15	v
2.2 Particle Chemistry	v
2.3 Multiple Particle Tracking	7
2.4 Isothermal Titration Calorimetry	9
3 EXPERIMENTAL MATERIALS & METHODS	12
3.1 Materials	12
3.1.1 Peptides	12
3.1.2 Tracer Particles	12
3.2 Methods	13
3.2.1 Multiple Particle Tracking	13
3.2.2 Isothermal Titration Calorimetry	13
4 RESULTS & DISCUSSION	1v
4.1 MAX1 Multiple Particle Tracking	1v
4.2 MAX1 Video Microscopy	18
4.3 Isothermal Titration Calorimetry	20
4.3.1 MAX1 ITC	20

4.3.2	MAX1 and HPL15 Comparison	29
4.3.3	pH Interactions in ITC	48
5	CONCLUSION	v0
Appendix		
A	PEPTIDE ADSORPTION CALCULATION	54
B	LANGMUIR EQUATION DERIVATION	56
C	SODIUM DODECYL SULFATE RESULTS	57
D	ACTIN RESULTS	59

LIST OF TABLES

2.1	Surface chemistry comparison between MAX1 and HPL15	5
2.2	Zeta potential measurements of the PS, COO, NH ₂ , and PEG particles.....	6
4.1	Binding enthalpies for MAX1-PS, COO, NH ₂ and PEG	22
4.2	Binding parameters for MAX1-PS, COO, and NH ₂	28
4.3	Binding enthalpies for HPL15-PS, COO, and NH ₂	38
4.4	Material pHs (and pK _a s) in nanopure water.....	48

LIST OF FIGURES

2.1	Proposed MAX1 folding and self-assembly process	4
4.1	Mean-squared displacement vs. lag time of 0.15 % MAX1 with 1 μm COO particles	16
4.2	Comparison of $\langle r(\tau) \rangle * a$ for variously sized PS and COO particles with 0.15% MAX1 at (A) $t = 6$ min and (B) $t = 30$ min	17
4.3	Video microscopy images of 0.15% MAX1 and particles approximately 12 minutes after self-assembly initiation	19
4.4	Measured signal for 0.175% MAX1 with PS and COO	21
4.5	$\Delta Q/\Delta X$ results for MAX1 with PS, COO, NH_2 and PEG	23
4.6	Total amount of absorbed heat for MAX1 with PS, COO, NH_2 and PEG	24
4.7	Total amount of absorbed heat normalized by ΔH_f for MAX1 with PS, COO, NH_2 , and PEG	25
4.8	Video microscopy images of 0.15% MAX1 and particles dispersed in water	27
4.9	Measured signal for 0.175% MAX1 and 0.08% HPL15 titrated in water	30
4.10	Measured signal for 0.175% MAX1 and HPL15 with PS	32
4.11	Measured signal for 0.175% MAX1 and HPL15 with COO	34
4.12	Measured signal for 0.126% MAX1 and 0.175% HPL15 with NH_2	36
4.13	$\Delta Q/\Delta X$ results for 0.175% HPL15 with PS, COO, and NH_2	37
4.14	ΔH_f comparison between MAX1 and HPL15	39
4.15	Total amount of absorbed heat for HPL15 with PS, COO, and NH_2	40
4.16	Total amount of absorbed heat for MAX1-PS and HPL15-PS	42

4.17	Total amount of absorbed heat for MAX1-COO and HPL15-COO	43
4.18	Total amount of absorbed heat for MAX1-NH ₂ and HPL15-NH ₂	45
4.19	Comparison of the amount of peptide adsorption to PS, COO and NH ₂ for MAX1 and HPL15	47
A.1	$\Delta Q/\Delta X$ results for (A) 64.15 mM SDS and (B) 128.5 mM SDS titrated in water (blank) and with PS	58
A.2	$\Delta Q/\Delta X$ results for actin with (A) PS and (B) BSA coated PS.....	60

ABSTRACT

Microrheological techniques characterize the rheological properties of a material by analyzing the thermal motion of small particles embedded within this medium. However, interaction between the embedded particles and the material is inevitable, and can lead to changes in the local environment surrounding the particles through adsorption or depletion. Such interactions may then lead to systematic errors in microrheological experiments. As microrheology is a relatively new technique, little quantitative knowledge is available on the effect these interactions have on such measurements. Thus, this thesis attempted to characterize and quantify the interactions occurring between two peptides, MAX1 and HPL15, and four particle types, polystyrene (PS), carboxylated polystyrene (COO), amine-modified polystyrene (NH₂) and polyethylene-glycol coated polystyrene (PEG). Multiple particle tracking (MPT) measurements were conducted with MAX1 and PS, COO, NH₂, and PEG particles to visualize the interactions occurring and to assess the effect these interactions have on observed viscoelastic properties. The non-overlapping mean-squared displacement curves observed using multiple particle tracking with MAX1 and variously sized PS and COO particles in a pH 9 buffer indicated surface chemistry interactions and the breakdown of the generalized-Stokes-Einstein relationship. Video microscopy images of MAX1 and PS, COO, NH₂, and PEG in pH 9 borate buffer indicated that the hydrophobic PS and COO particles were mono-dispersed and stable within the MAX1 medium, while the NH₂ and PEG particles clustered in the presence of

MAX1, indicating instability. To compare with MPT, Isothermal titration calorimetry (ITC) measurements were made with all peptides and particles to quantify the degree of peptide adsorption to probe particles by injecting the peptide into a cell containing microsphere particles. MAX1 with PS, COO, and NH₂ results were well fit with the Langmuir isotherm, suggesting simple adsorption kinetics, while MAX1 with PEG revealed more complicated interactions. HPL15 with PS, COO, and NH₂ results suggested complex mechanisms, and multi-layer peptide adsorption isotherms may more accurately describe these interactions than the simple Langmuir isotherm. All results shown here clearly indicate that characterization of these interactions is necessary in order to properly explain the dispersion and microrheological results. As such, the ITC experiments show allow for a better understanding of the interactions involved and the potential systematic errors arising from material-particle interactions from MPT measurements.

Chapter 1

MOTIVATION

Microrheology is used to quantify the viscous and elastic properties of complex fluids, and has the benefit of requiring very small quantities for sample analyses. Microrheology is often used to characterize the microstructure, micromechanics, and heterogeneities of biomaterials. Microrheological techniques characterize the rheological properties of a material by analyzing the thermal motion of small particles embedded within this medium. However, interaction between the embedded particles and the material is inevitable, and can lead to changes in the local environment surrounding the particles through adsorption or depletion. Such interactions may then lead to systematic errors in microrheological experiments.¹ While a few works have assessed these interactions on a qualitative basis, there is little quantitative knowledge available on these particle-material interactions.²⁻⁴ Thus, this thesis used Isothermal Titration Calorimetry (ITC) to quantify the degree of peptide adsorption to these particles, and determine whether these particle interactions are driven enthalpically or entropically. With a quantitative assessment of the interactions which result from particles with various

¹ Breedveld, V and D. J. Pine. *Journal of Materials Science* **2003**, 38, 4461-4470.

² McGrath, J. L; Hartwig, J. H; Kuo, C. *Biophysical Journal* **2000**, 79, 3258-3266.

³ Valentine, M. T. Surface Chemistry Effects for Microrheology. *Stanford University*. Sept 8, 2005.
<<http://www.stanford.edu/~mvalenti/megpeg.html>>

⁴ Valentine, M. T., Perlman, Z. E., Gardel, M. L., Shin, J. H., Matsudaira, P., Mitchison, T. J., and D. A. Weitz. *Biophysical Journal* **2004**, 86, 4004-4012.

surface chemistries, it should be possible to understand the effect these interactions have on microrheological measurements. In this way, the systematic errors resulting from these interactions may be more accurately accounted for. Thus, through a more thorough understanding of the interactions occurring between the particles and the material in which they are embedded, more accurate conclusions on a material's viscoelastic properties may be made from these microrheological measurements.

Chapter 2

INTRODUCTION

2.1 Peptide Structure and Chemistry

2.1.1 MAX1

Hydrogel networks have broad applications in tissue engineering and drug delivery.^{5,6} MAX1 is one such hydrogel which can be induced via a reversible self-assembly process through environmental changes such as a pH, temperature, ionic strength, electric field, and light changes.⁷⁻¹⁰ Consisting of twenty amino acid residues, MAX1 is an amphiphilic protein with a hydrophilic lysine face and a hydrophobic valine face.⁷ At neutral pH, the peptide yields an overall net positive charge. As shown in the schematic in Figure 2.1, this β -hairpin peptide begins intramolecular folding with the addition of a pH 9 borate buffer.⁸ Shortly thereafter, folding is followed by an intermolecular, and reversible, self-assembly process which results in a Max1 hydrogel network.⁸

⁵ Lee, K. Y.; Mooney, D. J. *Chem. Rev.* **2001**, *101*, 1869-1879.

⁶ Hoffman, A. S. *Adv. Drug Deliv. Rev.* **2002**, *43*, 3-12.

⁷ Schneider, J. P.; Pochan, D. J.; Ozbas, B.; Rajagopal, K.; Pakstis, L.; Kretsinger, J. *JACS* **2002**, *124*, 15030-15037.

⁸ Rajagopal, K.; Schneider, J. P. *Curr. Opin. Struct. Biol.* **2004**, *14*, 480-486.

⁹ Pochan, D. J.; Schneider, J. P.; Kretsinger, J.; Ozbas, B.; Rajagopal, K.; Haines, L. *JACS* **2003**, *125*, 11802-11803.

¹⁰ Ozbas, B.; Kretsinger, J.; Rajagopal, K.; Schneider, J. P.; Pochan, D. J. *Macromolecules* **2004**, *37*, 7331-7337.

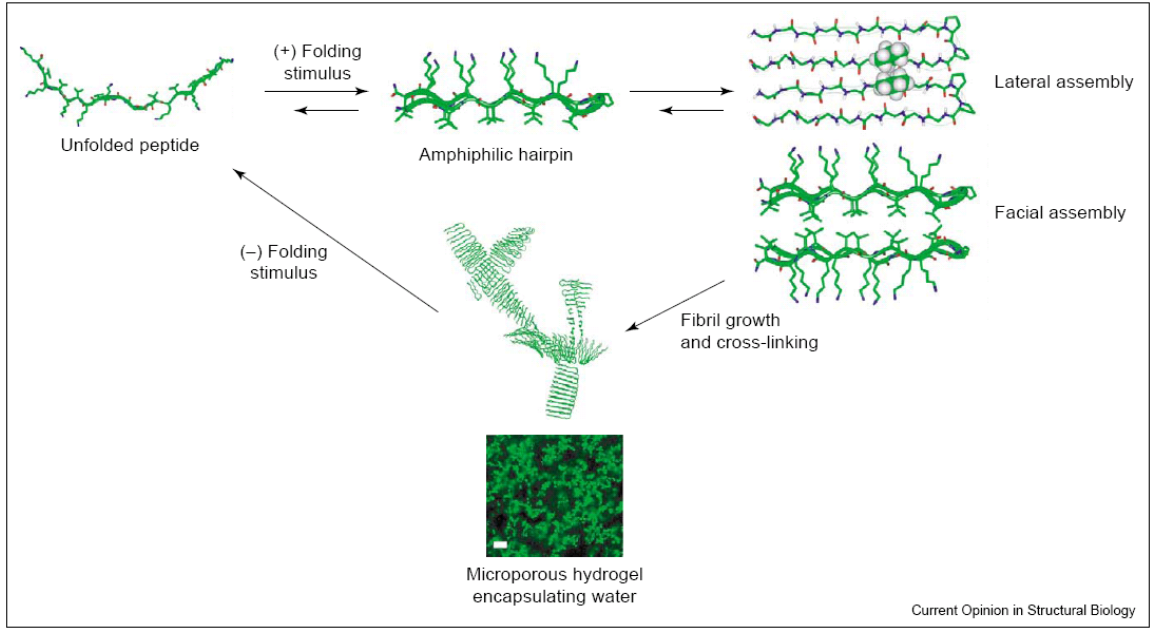
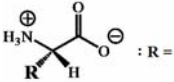
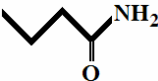


Figure 2.1. Proposed MAX1 folding and self-assembly process.⁸

Table 2.1. Surface chemistry comparison between MAX1 and HPL15.

Peptide	Point 15 Amino Acid	 : R =	pKa of Commonly Dissociated Hydrogen Ion
MAX1	Lysine		10.5
HPL15	Glutamine		---

2.1.2 HPL15

HPL15 is derived directly from MAX1, where the only difference between the peptides is that HPL15 has a one-point mutation of a lysine group to glutamine at point 15 (K15Q) of MAX1. HPL15 was chosen because it is very similar in structure to MAX1 and thus allowed us to see how small changes in the base material affect the quantitative analysis. Table 2.1 illustrates this comparison, where there are only two differences in surface chemistry between the two peptides. While both have an amine group on the terminal carbon, lysine has an additional carbon in this chain, and the terminal carbon in glutamine is a carbonyl group connected to amine, yielding a net neutral residue.

2.2 Particle Chemistry

Four similarly sized tracer particles with different surface chemistries were analyzed: fluorescent polystyrene (PS), carboxylated polystyrene (COO), amine-modified

Table 2.2. Zeta potential measurements of the PS, COO, NH₂ and PEG particles.

Microsphere Type	Zeta Potential in 10 mM NaCl [mV]	Zeta Potential in pH 9 borate Buffer [mV]
PS	-102 +/- 7.3	-67.3 +/- 13.5
COO	-97.2 +/- 9.4	-62.0 +/- 13.0
NH ₂	-49.0 +/- 7.7	-28.1 +/- 10.3
PEG	-22.2 +/- 4.9	-11.8 +/- 11.2

polystyrene (NH₂), and polyethylene glycol coated polystyrene (PEG). PS particles have a hydrophobic surface with negatively charged alkyl sulfonates, and sulfates.¹¹ COO particles are also hydrophobic with additional negative charges from its carboxyl groups, making them less hydrophobic than PS particles. Both PS and COO have the ability to bind strongly to any molecule with hydrophobic character, including proteins, nucleic acids and many small biomolecules.¹² NH₂ particles are amphiphilic with positively charged amine groups (in addition to the negatively charged sulfate groups) yielding a high charge density.¹² PEG particles are also hydrophilic, and its coating is intended to resist protein adsorption. Resistance due to steric repulsion effects arise from its loss in conformational entropy and the unfavorable desolvation of the polymer chains as the polymer layer expels water molecules.¹³ These particle types, which bear different affinities for peptide adsorption due to their unique surface chemistries, may yield different local viscoelastic responses from the medium in which

¹¹ Polystyrene Microspheres: Frequently Asked Questions. Polysciences, Inc. **238**.

¹² Working with FluoSpheres Fluorescent Microspheres: Properties and Modifications. *Molecular Probes* (2004). <http://probes.invitrogen.com/media/pis/mp05001.pdf>

¹³ Gardel, M.L; Valentine, M.T.; and Weitz, D.A. Microrheology. *Microscale Diagnostic Techniques*, ed. Kenny Breuer. New York: Springer-Verlag **2005**.

they are embedded.¹³ Zeta-potential measurements yielded the net surface potential of each tracer particle in two solutions.¹⁴ The ζ -potential results are shown in Table 2.¹⁴

2.3 Multiple Particle Tracking

The mechanical properties of scaffolds have been found to be a key variable in facilitating cell growth. Because a suitable environment in which cells prosper is an essential component in developing these artificial scaffolds, it is crucial to determine the microrheological properties of potential scaffold materials, such as MAX1. The mechanical response at the macroscopic level has been characterized with 2% MAX1 using bulk rheological techniques.⁹⁻¹⁰ However, little is known about its responses at the microscopic level. Multiple particle tracking with fluorescent tracer particles serves as an excellent method to characterize these microrheological properties.^{15,16,17} Responses are measured locally and the surrounding MAX1 environment can then be inferred by measuring the mean-squared displacement, $\langle \Delta r^2(x, \tau) \rangle$, for each probe particle over a series of images. To do this, a “movie” is created by taking 500 images in series. The gelation kinetics of MAX1 are tracked by taking several movies over the course of the self-assembly process. Within each movie, the trajectory of each particle is found and the displacement is determined as a function of the lag time, τ , using an image analysis

¹⁴ Veerman, C.; Gable, B.E. Rajagopal, K.; Schneider, J.P.; Furst, E.M. *Submitted for publication* **2006**.

¹⁵ Mason, T. G.; Weitz, D. A. *Physical Review Letters* **1995**, *74*, 1250-1253.

¹⁶ Mason, T. G.; Ganesan, K.; Zanten, J. H. v.; Wirtz, D.; Kuo, S. C. *Phys. Rev. Lett.* **1997**, *79*, 3282-3285.

¹⁷ Schnurr, B.; Gittes, F.; MacKintosh, F. C.; Schmidt, C. F. *Macromolecules* **1997**, *30*, 7781-7792.

routine (IDL software package).¹⁸ The mean-squared displacement of all particles over each movie is found by averaging the displacements of all particles as a function of τ . For fluid-like systems such as water, the mean-squared displacement of the particles presents information about the surrounding environment via the following equation,

$$\langle \Delta r^2(\tau) \rangle = 2dD\tau \quad (1)$$

where d is the number of dimensions and D is the diffusion constant. In this equation, the Stoke-Einstein relation is valid when assuming a no-slip boundary condition in the limit of a freely diffusing particle,

$$D = \frac{k_B T}{6\pi\eta a} \quad (2)$$

where k_B is the Boltzmann constant, T is temperature, η is viscosity, and a is the particle radius.¹³ Thus, images, taken using a microscope with a CCD camera, yield measurements of $\langle \Delta r^2 \rangle$ as a function of lag time. This provides both the material diffusion coefficient and viscosity. From the mean-squared displacement measurements, the material viscoelastic response can be calculated using the Generalized Stokes-Einstein Relation (GSER).

$$\tilde{G}_1(s) = \frac{k_B T}{as\pi \langle \Delta \tilde{r}^2(s) \rangle} \quad (3)$$

However, this relationship holds only when a no-slip boundary condition exists between the material and the particles embedded within it. This relationship depends on the local material structure and, as a result, the interactions between the particles and the medium.

¹⁸ Crocker, J. C.; Grier, D. G. *Journal of Colloid and Interface Science* **1996**, *179*, 298-310.

In order to accurately characterize complex materials using microrheological techniques, the interactions between the tracer particles and material must also be characterized.¹³

The proper characterization of the effects of the tracer particle surface chemistry on the material network is necessary in order to accurately interpret multiple particle tracking experiments.¹³

2.4 Isothermal Titration Calorimetry

To study particle-peptide interactions, isothermal titration calorimetry (ITC) was used to quantify the degree of peptide adsorption to probe particles. Typically, ITC is used to examine protein-ligand interactions, where a ligand is injected into a sample cell containing a protein. However, such experiments are useful in this research because ITC experiments are capable of measuring the heats of binding by observing the enthalpy changes upon isothermal changes in solution, which allows us to quantify the amount of peptide adsorbed to particle surfaces. In this work, the peptide solution was injected into a cell containing a selected type of microsphere particles. As the peptide is injected into the particle solution, the heat change upon interaction between the peptide and particles is measured directly.¹⁹ Because the heat absorbed or released is directly proportional to the amount of peptide binding to the particle surface when no other heats are present, this technique enables us to quantify the degree of peptide adsorption to these particles, provided that the heat per peptide-particle interaction does not change. From this, the

¹⁹ What is ITC? *MicroCalorimetry*. <http://www.microcalorimetry.com/index.php?id=13>

individual binding affinities, K_a , binding enthalpies, ΔH_f , and binding isotherms can be determined, provided one has a reasonable adsorption model.²⁰

The resulting output from each experiment is the feedback power required to maintain a constant temperature difference between the reference and sample cell, P [mcal/s], versus time [s]. Thus the heat absorbed or released in each injection, $\frac{\Delta Q}{\Delta X}$ [cal/mol], can be determined by integrating the area underneath each injection peak, and by subtracting the appropriate blank titration of both the peptide and particle solution alone with the solvent.²⁰ The binding enthalpies are then found by extrapolating this integrated data to the theoretical heat evolved at zero peptide concentration. From this information, the total heat absorbed or released for a given concentration, Q [μ cal], can then be determined by using the following relationship, where C_i is the cell concentration after injection I, and ΔV_i is the volume of injection i.

$$Q = \sum_{i=1}^{injections} \left(\frac{\Delta Q}{\Delta X} \right)_i (C_i - C_{i-1}) \Delta V_i \quad (4)$$

If a binding isotherm is known (or assumed) for a given peptide-particle interaction, this total heat can be related to its binding affinity. Assuming simple, monolayer adsorption, the binding can be described by the Langmuir adsorption isotherm. Equation (5) uses the Langmuir isotherm to relate the total heat data to the particles' binding affinities (assuming the free peptide concentration is that of the total peptide concentration within the cell).

²⁰ Leavitt, S.; Freire, Ernesto. *Current Opinion in Structural Biology* **2001**, 11, 560-566.

$$Q(P_T) = \Delta H_f \left(\frac{K_a [P_T] [S_T]}{1 + K_a [P_T]} \right) \quad (5)$$

In this equation, ΔH_f refers to the binding enthalpy, P_T refers to the total peptide concentration in the cell, and S_T is the total number of binding sites present. With both the binding enthalpy and binding affinity known, the entropic contribution of the peptide-particle interaction, ΔS_f , as well as the free energy associated with this reaction, ΔG_f , can be determined from Equation (6),

$$\Delta G_f = -RT \ln K_a = \Delta H_f - T\Delta S_f \quad (6)$$

where T is the absolute temperature. Thus, ITC allows the determination of the enthalpic and entropic contributions involved in peptide adsorption when regressed to a physically plausible adsorption isotherm.

Chapter 3

EXPERIMENTAL MATERIALS & METHODS

3.1 Materials

3.1.1 Peptides

Both MAX1 and HPL15 were provided by the Schneider group in the Chemistry Department at the University of Delaware. The hydrogel network formation for the MAX1 Multiple Particle Tracking experiments was prepared by dissolving lyophilized MAX1 with milli-Q water, followed by the addition of a pH 9 borate buffer (125 mM borate and 10 mM NaCl), which initiated self-assembly.

3.1.2 Tracer Particles

The tracer particles used were fluorescent polystyrene and carboxylated polystyrene from Polysciences, Inc (Warrington, PA), and amine-modified polystyrene from Molecular Probes (Carlsbad, CA). Polyethylene glycol coated polystyrene particles were prepared from the amine-modified particles as follows. The NH₂ particles were washed and redissolved in milli-Q water, and a succinimidyl ester of PEG propionic acid was covalently coupled to these particles to obtain the PEG particles. Three diameters of the polystyrene particles, 0.5, 0.75, and 1 μm, and two diameters of the carboxylated

particles, 0.75 and 1 μm , were used in the Multiple Particle Tracking experiments. ITC experiments used 1 μm PS, COO, NH_2 and PEG particles.

3.2 Methods

3.2.1 Multiple Particle Tracking

Each measured sample consisted of tracer particles with a final volume fraction of 0.4%, protein with a final volume fraction of 0.15%, and a pH buffer of 7, 8, or 9 with a 1:1 final volume ratio. The final sample volume was 300 μL , and time zero began with the addition of the pH 9 buffer, which induced the self-assembly process. 45 μL of the sample was injected between a microscope slide and a cover slip, and joined via an adhesive spacer and UV curing epoxy glue. A CCD camera attached to an inverted optical epifluorescence microscope (Axiovert 200, Zeiss, N.A. 0.75) captured 500 images per measurement, with a temporal resolution of approximately 60 Hz and at a total magnification of 64x. Approximately ten measurements were taken for each sample at various times throughout the gelation process. The images recorded were then analyzed using a particle tracking routine, IDL, which selected and linked suitable particles, and determined their displacements over all frames. $\langle \Delta r^2(\tau) \rangle$ was then calculated as a function of lag time using a custom matlab routine.¹⁸

3.2.2 Isothermal Titration Calorimetry

ITC measurements were carried out in a VP-ITC instrument at 25°C (Microcal LLC, Northampton MA). 0.08%, 0.13%, and 0.175% (0.246 mM, 0.385 mM, and 0.539

mM) MAX1 and HPL15 were titrated into 0.2% microspheres, or approximately 10^{11} particles per samples, for 1 μ m PS, COO, NH₂, PEG. Each experiment involved 25 injections of 10 μ L peptide samples, each lasting 20 seconds, with a mixing speed of 260 rpm. At least ten minutes were allotted between injections to allow time for equilibration. From this, the heat released or absorbed from each injection was measured. Dilution effects were taken into account by two sets of blank titrations, where water was injected into 0.2% microspheres, and the peptide solutions were injected into water. The amount of heat released or absorbed from each blank titration was then subtracted from the aforementioned injection peaks. The individual binding constants, K_a , binding enthalpies, ΔH_f , and binding isotherms were then determined from these final injection peaks, where applicable.

Chapter 4

RESULTS & DISCUSSION

4.1 MAX1 Multiple Particle Tracking

0.15% MAX1 samples with 0.5, 0.75, and 1 μm PS and 0.75, and 1 μm COO tracer particles were analyzed. For all experiments, the particle mean-squared displacement decreased with increasing time of gelation. Figure 4.1 depicts this, where the mean-squared displacement of the 1 μm COO particles is closest to that of purely viscous diffusion in water initially, and decreases as time passes. As the particles are trapped within the forming MAX1 hydrogel, the fluorescent particle mobility is increasingly restricted regardless of the probe surface chemistry or size. A comparison of the variously sized PS and COO particles in the MAX1 medium 6 minutes after the self-assembly process is shown in Figure 4.2A, where the differences in particle diameter, a , have been accounted for by multiplying $\langle \Delta r^2(\tau) \rangle$ by a . Figure 4.2A indicates that the mean-squared displacements with the various particle sizes and surface chemistries are nearly indistinguishable initially, suggesting a potential independence of probe size and surface chemistry. However, Figure 4.2B, which shows the mean-squared displacements 30 minutes after the self-assembly initiation, indicates a very different scenario. Although the differences in particle sizes are still accounted for, the curves at 30 minutes no longer

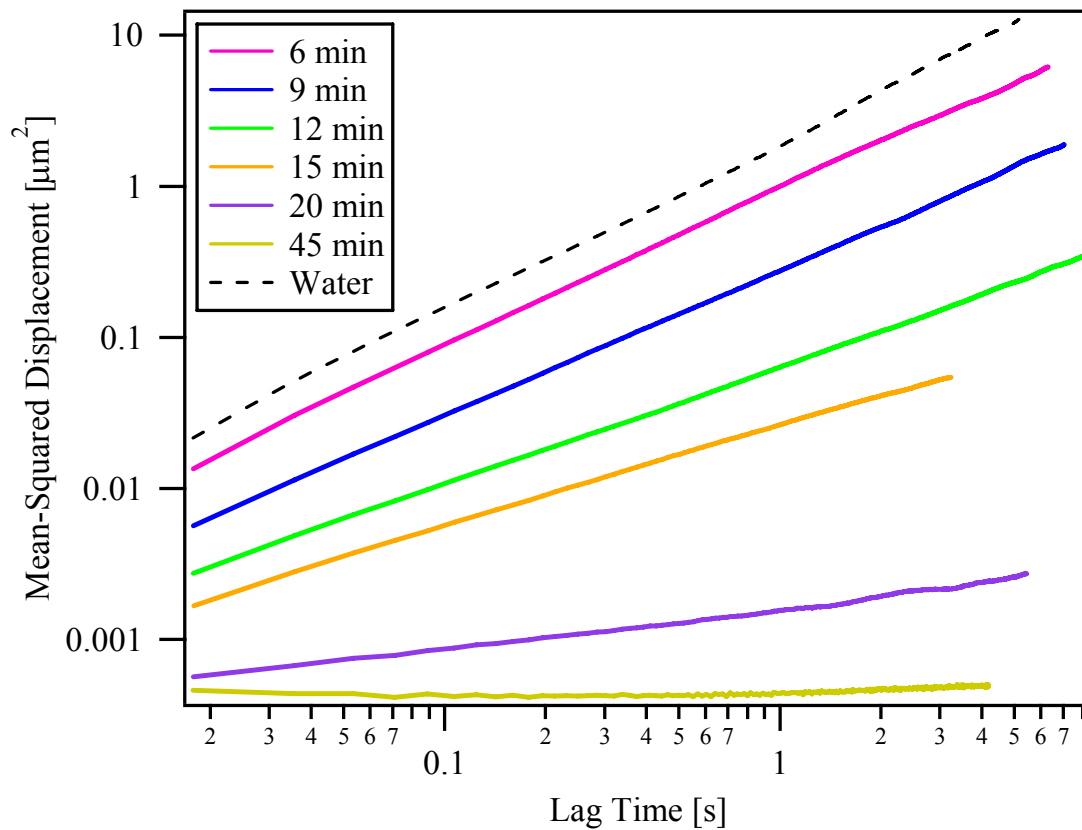


Figure 4.1. Mean-squared displacement vs. lag time of 0.15% MAX1 with 1 μm COO particles. Each colored curve represents a given time following the buffer addition ($t = 0$ min).

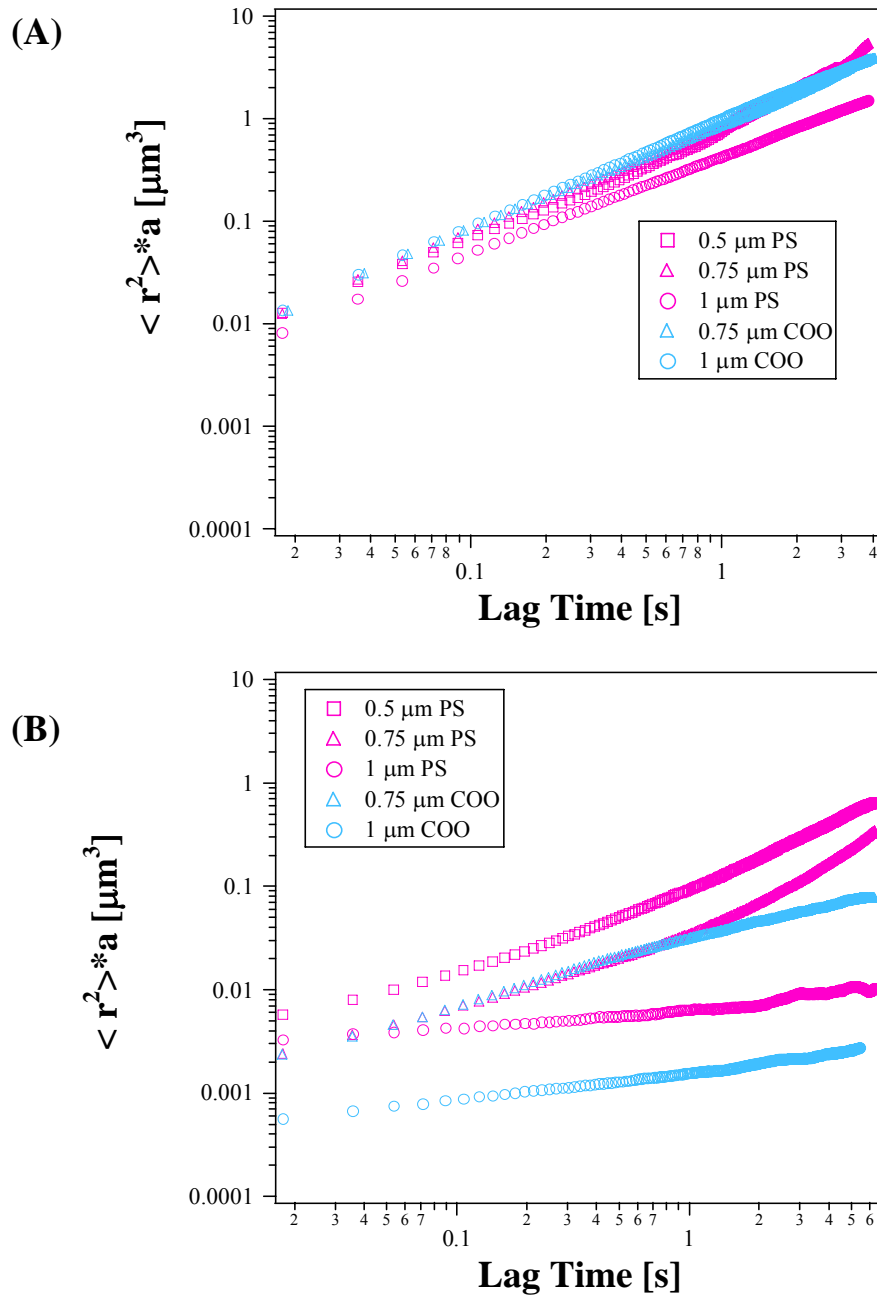


Figure 4.2. Comparison of $\langle r(\tau) \rangle * a$ for variously sized PS and COO particles with 0.15% MAX1 at (A) $t = 6$ min and (B) $t = 30$ min.

overlap. This indicates the breakdown of the GSER because the mean squared-displacement does not exhibit $1/a$ behavior. The anomalous nature of these curves strongly suggests surface chemistry interactions between the particles and MAX1.

4.2 MAX1 Video Microscopy

As mentioned, multiple particle tracking of MAX1 with variously sized PS and COO particles indicated unique surface chemistry interactions between the protein and particles. With this interaction revealed by these microrheological measurements, video microscopy images were taken with MAX1 and the hydrophobic PS and COO particles, as well as with the hydrophilic NH₂ and PEG particles. Figure 4.3 shows the resulting images with MAX1 and 1 μm PS, COO, NH₂, and PEG particles in pH 9 borate buffer at approximately 12 minutes after self-assembly initiation. Figure 4.3 reveals a strong distinction between the hydrophobic and hydrophilic particles. The PS and COO particles are dispersed in the MAX1, while the NH₂ and PEG particles form clusters in the presence of MAX1. This result seems logical when realizing that peptides and proteins are more likely to adsorb to hydrophobic rather than hydrophilic particles (which are known to withstand protein adsorption). Thus, the hydrophobic PS and COO particles may remain stable and mono-dispersed within the MAX1 medium because they are interacting directly with this medium. Conversely, the hydrophilic NH₂ and PEG particles experience particle clustering due perhaps in part to the lack of interaction occurring between MAX1 and the particles, which leads to depletion interactions which drive the particles to cluster.

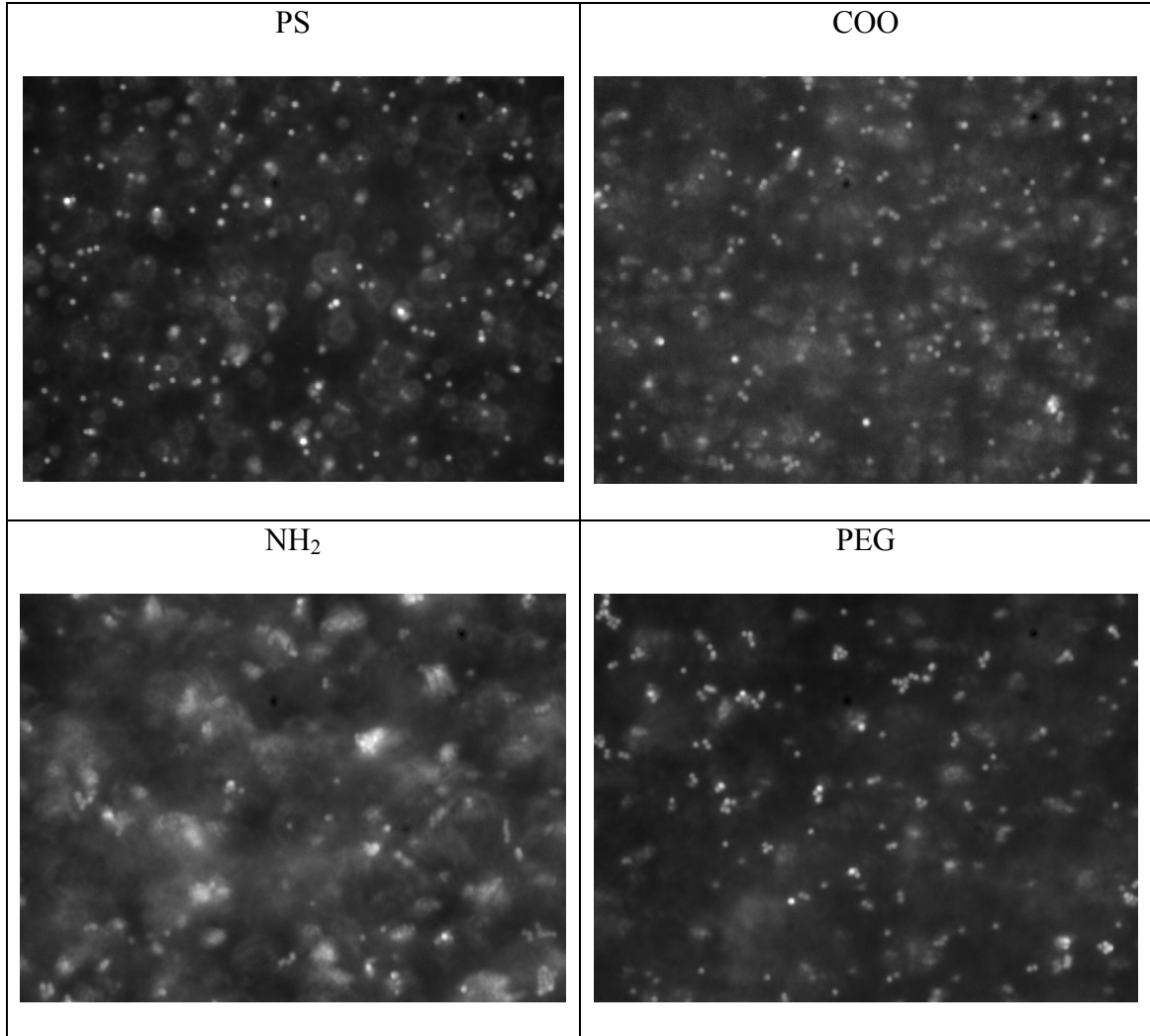


Figure 4.3. Video microscopy images of 0.15% MAX1 and particles approximately 12 minutes after self-assembly initiation.

4.3 Isothermal Titration Calorimetry

With the Multiple Particle Tracking and Video Microscopy visualizations of the different interactions occurring between MAX1 and the particles with various surface charges, the degree of peptide adsorption was characterized quantitatively using isothermal titration calorimetry. ITC is a thermodynamic technique for monitoring any chemical reaction initiated by the addition of a binding component.¹⁹ (The following analysis currently assumes no heat evolved from protonation-deprotonation).

4.3.1 MAX1 ITC

ITC experiments were conducted with MAX1 and PS, COO, NH₂ and PEG particles to quantify the degree of peptide adsorption on the particles. A comparison of these interactions between the different particles yields insight on the effect surface chemistry plays on these interactions. Figure 4.4 shows the measured signal corresponding to the power necessary to maintain a constant temperature difference between the reaction and reference cells as 0.175% MAX1 was injected into 0.2% PS and COO particles. These upward peaks for each injection point were observed for all four particle types, and they correspond to an increased feedback power necessary to maintain a constant temperature difference.²¹ The upward peaks also signify that endothermic interactions are taking place, which indicates entropically driven binding.²² The absorbed heat from each injection corresponds to the area integrated under each injection peak.

²¹ Holdgate, G.A.; Ward, W. H.J. *Drug Discovery Today* **2005**, 10, 1543-1550.

²² Lecture 6: Isothermal Titration Calorimetry. *University of Utah –Dept. of Biochem.*
<https://wasatch.biochem.utah.edu/wes/teachfiles/Lecture6/Lecture%206.pdf>

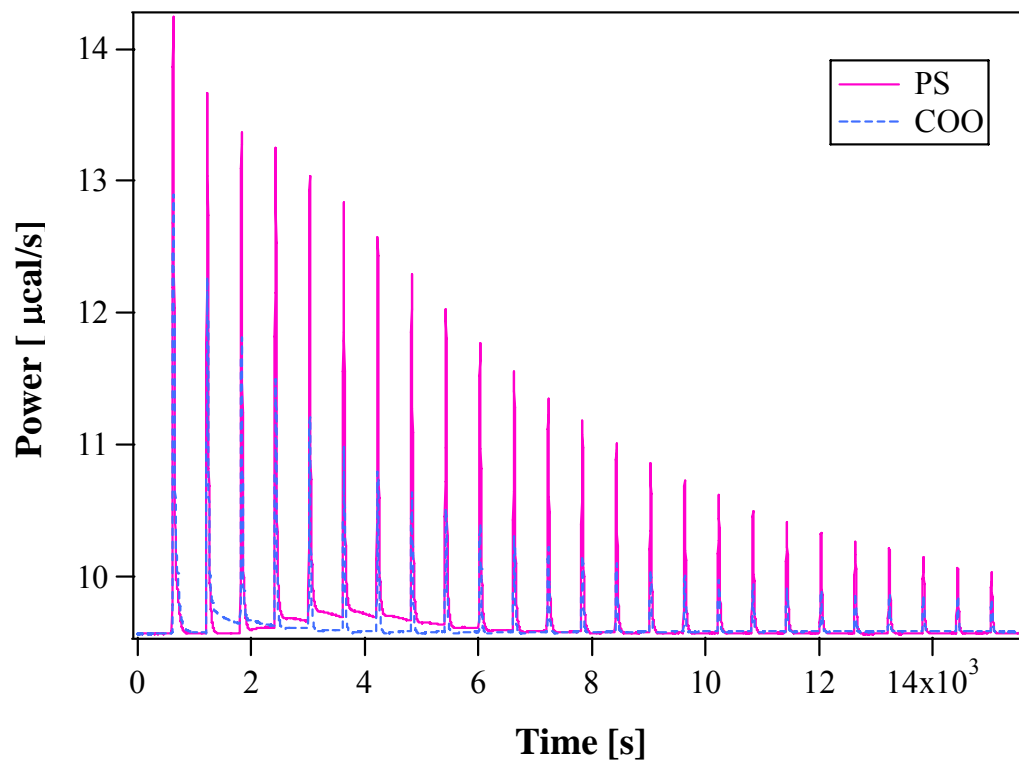


Figure 4.4. Measured signal for 0.175% MAX1 with PS and COO. Each peak corresponds to addition of 10 ml at each injection point.

Table 4.1. Binding enthalpies for MAX1-PS, COO, NH₂ and PEG.

	PS	COO	NH₂	PEG
ΔH_f [kJ/mol]	130.4 +/- 12.9	203 +/- 16.0	182.7 +/- 59.0	*123.7 +/- 0.79

**This heat is not ΔH_f , but a combination of self interactions and interactions with MAX1*

Thus, integration of these peaks yields the total heat per mole of injectant as a function of the peptide concentration. Figure 4.5 shows the result of this integration after subtracting both the peptide and particle blank titrations. Figure 4.5 clearly shows different binding affinities for MAX1 with the different surface chemistries of the particles, as indicated by the non-overlapping curves. The binding enthalpies are found by extrapolating this integrated data to the theoretical heat evolved at zero peptide concentration using linear fits of the 2-4 data points (the first data point being excluded, as it usually considered inaccurate due to initial dilution effects). Table 4.1 shows the result of this extrapolation. Using this integrated data in conjunction with Equation (4), we arrive at the total heat absorbed as a function of the peptide concentration in Figure 4.6. Figure 4.6 reveals that the MAX1-PS interactions experience the largest heat evolved, followed by MAX1-PEG, MAX1-COO, and the least heat evolved corresponds to the MAX1-NH₂ interactions. Figure 4.7 accounts for the differences in the binding enthalpies of the different interactions by normalizing Q with these ΔH_f values. Figure 4.7 is more representative of the degree of peptide adsorption because it accounts for the differences in binding heats. This result reveals the same trend as seen in Figure 4.6. The PS, COO and NH₂ results were expected in that the hydrophobic PS and COO particles should experience the

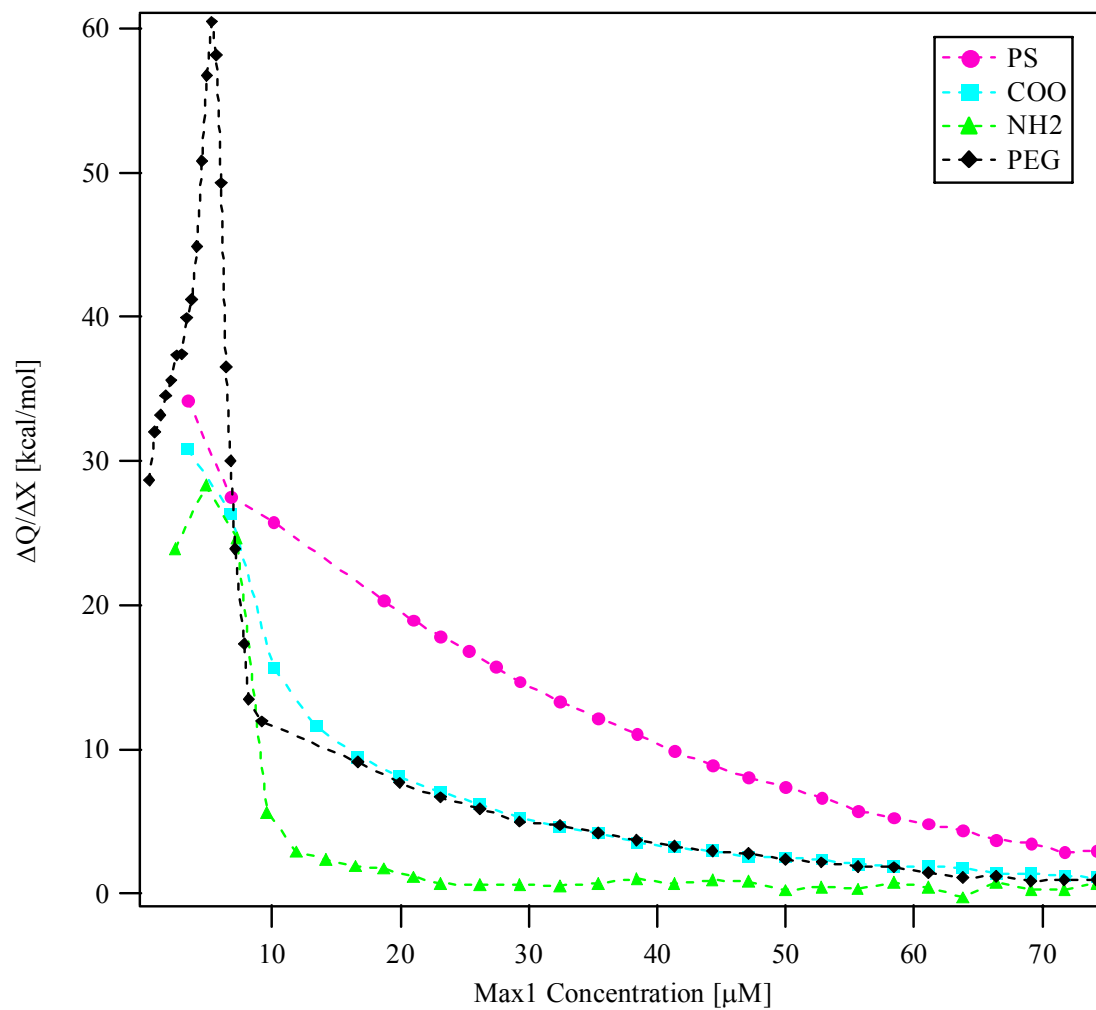


Figure 4.5. $\Delta Q/\Delta X$ results for MAX1 with PS, COO, NH₂ and PEG.

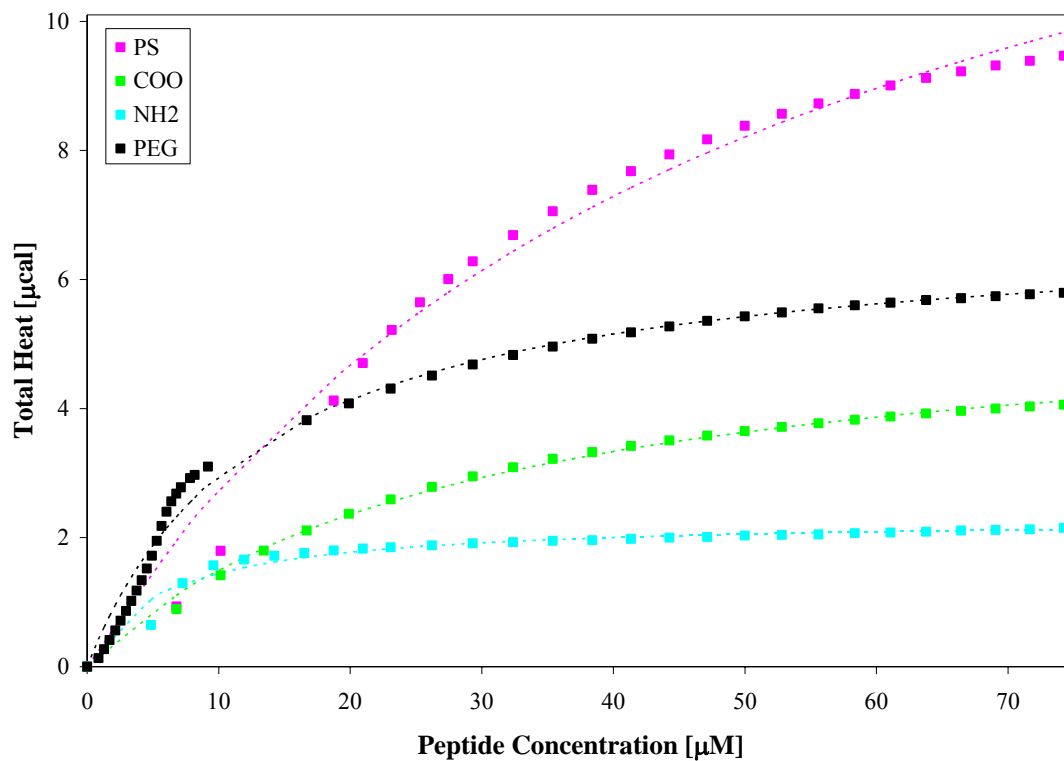


Figure 4.6. Total amount of absorbed heat for MAX1 with PS, COO, NH₂ and PEG. Langmuir fits shown as dotted lines.

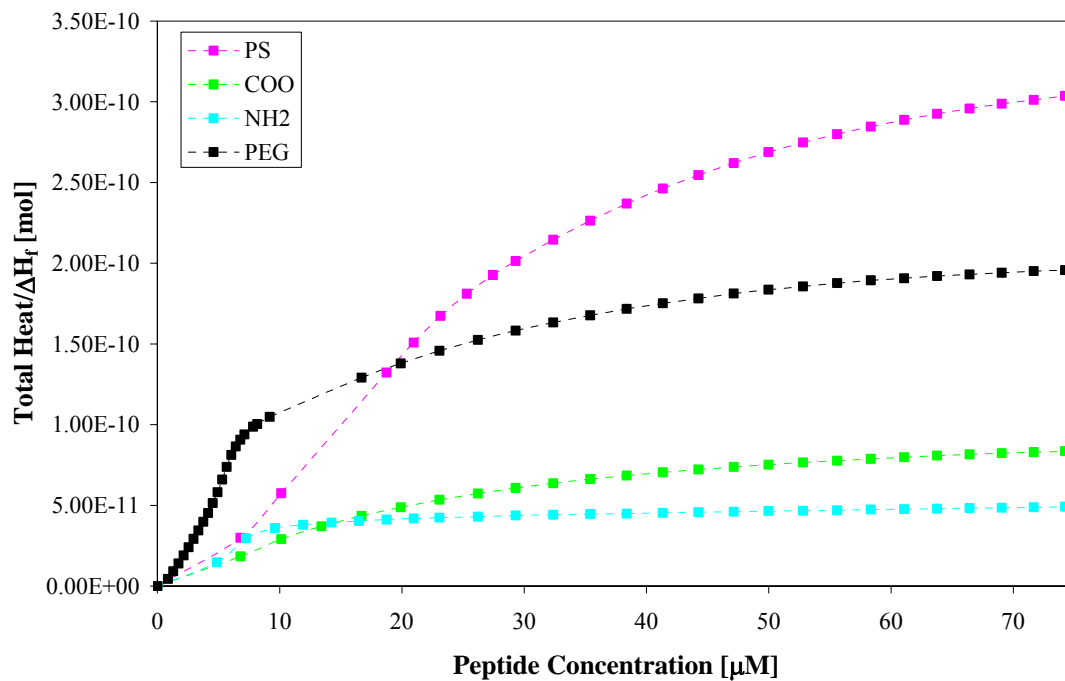


Figure 4.7. Total amount of absorbed heat normalized by ΔH_f for MAX1 with PS, COO, NH₂, and PEG. (Dashed lines just illustrative – no fits_

largest degree of peptide adsorption, while the hydrophilic NH₂ particles experience a minimal degree of peptide adsorption. This is most logical when considering the surface charges, where MAX1 has a net positive surface charge, whereas the PS and COO particles have a high net negative charge. This leaves many free adsorption sites, facilitating a large degree of peptide adsorption. Conversely, the NH₂ particles have a much weaker net negative charge which allows for less peptide adsorption with fewer free adsorption sites. Conversely, PEG, which has the weakest negative charge, would be expected to experience the smallest peptide adsorption. However, Figure 4.6 shows larger amounts of heat absorbed for the PEG particles than both the COO and NH₂ particles. To yield some insight on this perhaps unexpected MAX1-PEG result, video microscopy images were taken with all four particles types in the presence of MAX1 in water. While the PS, COO, and NH₂ particles did not experience particle clustering, Figure 4.8 shows the interactions occurring with MAX1 and PEG. Figure 4.8 indicates PEG particle clustering in the presence of MAX1 (no buffer), which mimics conditions of the ITC measurements. Thus the large degree of heat absorbed from the ITC measurements may not only be the result of MAX1 adsorption, but rather, a combined effect of peptide adsorption and initial PEG clustering in the presence of MAX1. The large peak observed in Figure 4.5 occurs at low concentrations, which corresponds to the initial introduction of MAX1 into the sample cell containing the PEG solution. Thus, the initial addition of MAX1 may create initial PEG clustering that the ITC measurements detect, and once the particles become stable and the clustering ceases, the minimal peptide adsorption results. In other words, once the particles cluster initially to become stable in the new MAX1

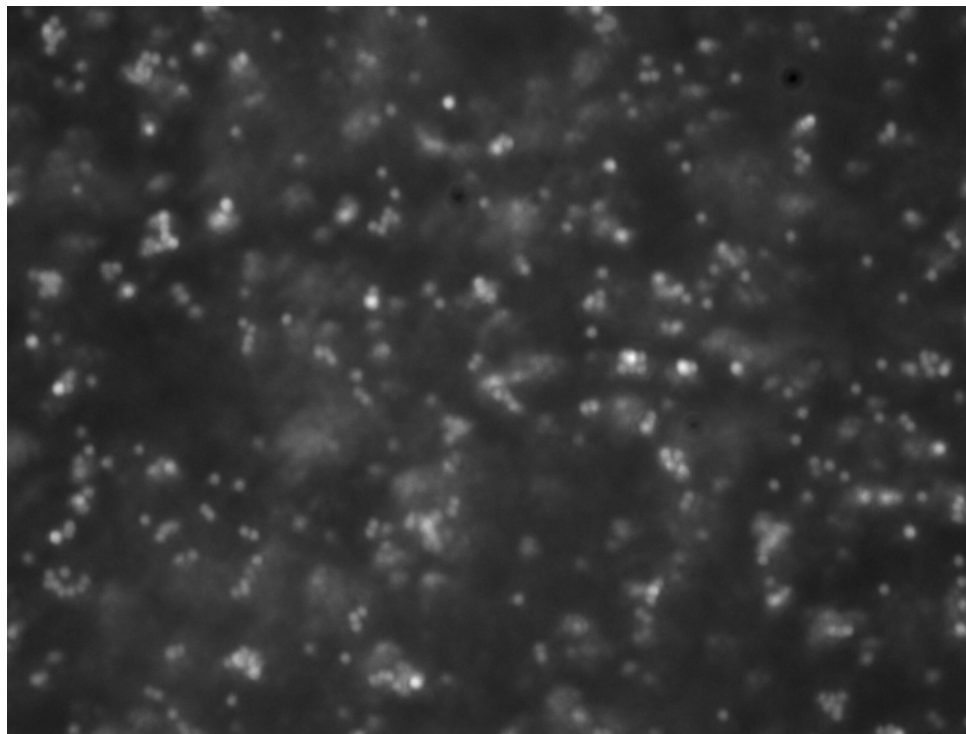


Figure 4.8. Video microscopy images of 0.15% MAX1 and particles dispersed in water.

Table 4.2. Binding parameters for MAX1-PS, COO, and NH₂.

	ΔH_f [kJ/mol]	S_T [fmol]	K_a [m ³ /mol]	ΔG_f [kJ/mol]	ΔS_f [kJ/ K mol]
PS	130.4 +/- 12.9	27.16	16.76 +/- 1.47	-6.84	0.461
COO	203.0 +/- 16.0	3.29	39.65 +/- 1.75	-8.92	0.711
NH₂	182.7 +/- 59.0	0.31	168.92 +/- 17.23	-12.44	0.655

environment, the clustering ceases and the heat measured thereafter corresponds to the peptide adsorption to the particles. Thus, where Table 4.1 shows that the PEG particles have the least amount of heat absorbed during binding, it must be realized that this ΔH_f may not only relate to the heat of adsorption, but also the heat involved in particle clustering.

With the total heat as a function of peptide concentration known, the Langmuir isotherm was used to fit this data by using Equation (5). Although the PEG particles were fit using the Langmuir assumptions, the binding affinity calculated using this method was unreliable because these MAX1-PEG interactions suggested a more complex mechanism than that defined by a Langmuir Isotherm. The corresponding fits are shown by the dashed lines in Figure 4.6. As can be seen in the figure, the PS, COO and NH₂ curves fit well with the experimental data. From this, the PS, COO, and NH₂ binding affinities were found through Equation (5), assuming ΔH_f was independent of the extent of MAX1 adsorption. ΔG_f and ΔS_f were then found using Equation (6). The resulting values from these calculations are shown in Table 4.2. This table shows that PS has the greatest number of adsorption sites, followed by COO, and NH₂. This result is expected in that PS

has the most negatively charged units that MAX1 could adsorb to, whereas the NH₂ particles has the least negative net charge, which leaves fewer units for MAX1 to adsorb to. Interestingly, the NH₂ particles actually have the strongest binding affinity to MAX1, followed by the COO and PS particles. With the NH₂ particles having the strongest affinity for MAX1 it makes sense that the binding has the most favorable free energy change. These results suggest that if the particles would have an identical number of binding sites, the NH₂ particles would actually experience the greatest peptide adsorption.

4.3.2 MAX1 and HPL15 Comparison

As seen, the MAX1 ITC results were reasonably straightforward; the simple Langmuir isotherm could be fit to the PS, COO and NH₂ data with reasonable accuracy. However, when the MAX1 peptide sequence was slightly altered so that the lysine at point 15 was substituted with a glutamine group, very different behavior was observed. This section compares the MAX1 results to the HPL15 results to show the differences in particle-peptide interaction that result from a single one-point mutation to a Lysine residue on a 20 amino acid long peptide.

Figure 4.9 shows the feedback power corresponding to the blank titration of the peptides into water. This figure shows the expected dilution effect and heat of mixing for the MAX1 peptide, where a decrease in feedback power is required as the sample cell peptide concentration increases with each injection. Both MAX1 and HPL15 release heat initially, which corresponds to the downward pointing peaks. However, while heat is continually released with the MAX1 injections, the HPL15 behavior is unexpectedly

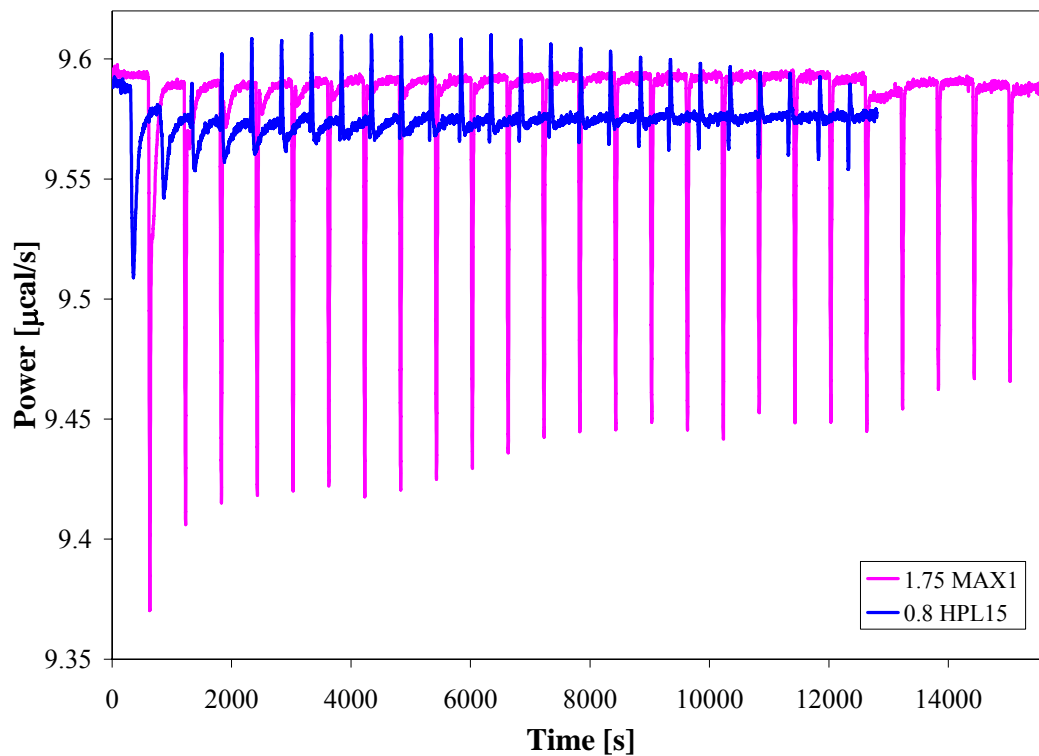


Figure 4.9. Measured signal for 0.175% MAX1 and 0.08% HPL15 titrated in water.

different. In the HPL15 case, the peaks actually change sign. In other words, heat is no longer released, but is instead absorbed as more HPL15 peptide is added to the solution. This result suggests that the MAX1 peptide does not experience strong interactions with itself, whereas HPL15 interacts with itself upon reaching a certain concentration (approximately 0.06 mM in this case). This result suggests that the Langmuir isotherm cannot be used with the HPL15 data. The Langmuir isotherm assumes monolayers of the peptide on the particle surfaces, and because HPL15 has the potential to interact with itself, it is likely that the peptide will form multiple layers on the particle surfaces.

Keeping these unique peptide interactions in mind, the HPL15 peptide was titrated into each of the particle types. Figure 4.10 shows the raw data corresponding to both MAX1 and HPL15 injected into a PS solution. This figure shows that more heat is required to maintain a constant temperature between the sample and reference cell for the MAX1-PS interactions than the HPL15-PS interactions (approximately 4.1 and 3.5 $\mu\text{cal/s}$ for the first two peaks). Thus, even the slight decrease in the overall net positive charge of the peptide appears to decrease the interactions occurring between the peptide and particles. In addition to the differences in heat absorbed, the peptide interactions are also drastically different. The MAX1-PS interaction is strongest initially, and decreases as more peptide is added. This makes sense in that as the number of adsorption sites on the PS surfaces decreases, less peptide can adsorb to the particles. Conversely, the HPL15 may initially experience more peptide adsorption to the particles with the addition of peptide. This interaction may then experience a maximum saturation point, and then the

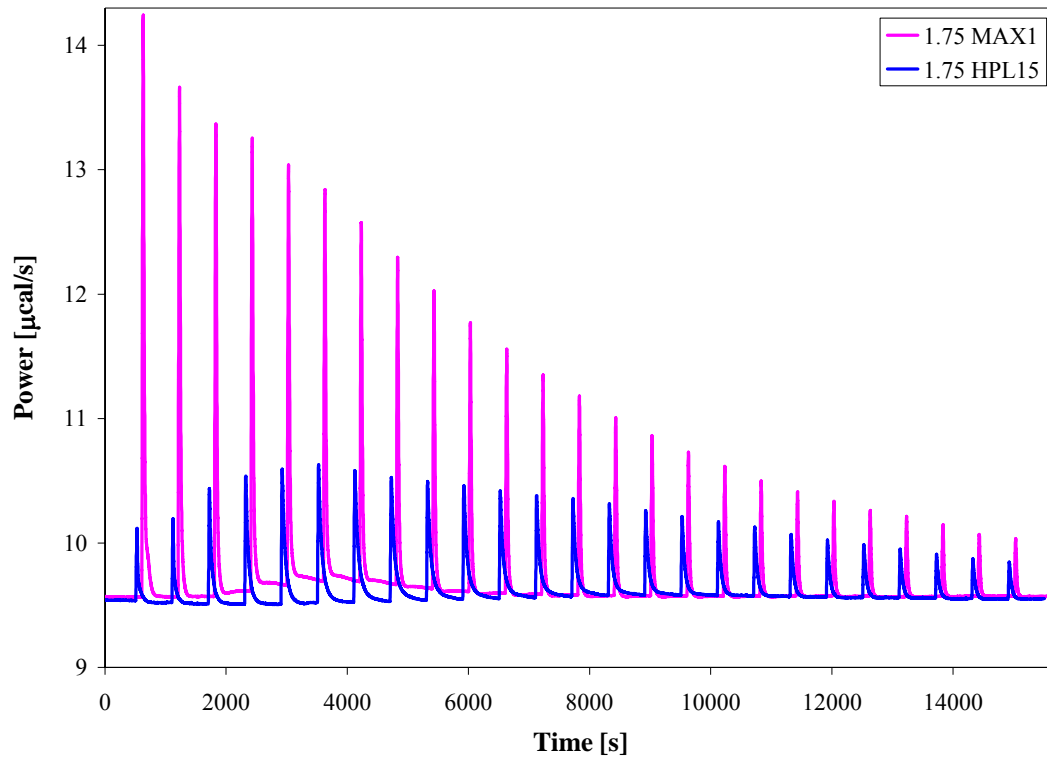


Figure 4.10. Measured signal for 0.175% MAX1 and HPL15 with PS.

peptide adsorbs less to the particles as the concentration increases. This discrepancy may be explained by a competition of HPL15 between adsorption to the particles and self interactions. Regardless, the unique HPL15-PS interactions certainly experience a complex adsorption mechanism that will require further investigation for more insight.

The interactions between MAX1-COO and HPL15-COO were then compared, and the raw data corresponding to this is shown in Figure 4.11. Figure 4.11A shows a similar trend to the PS interactions, where the MAX1-COO peaks are much stronger than the HPL15-COO peaks, indicating that less heat is required to maintain a constant temperature difference between the sample and reference cells (approximately 3.1 and 2.6 $\mu\text{cal/s}$ for the first two peaks). The MAX1-COO curve has strong peaks and an expected decrease in adsorption as more peptide is added and the binding sites are being filled. The HPL15-COO interactions are more clearly visualized in Figure 4.11B. The first two peaks of the HPL15-COO curves correspond to this trend, where the second peak is weaker than the first peak. As seen in this figure, the peaks are no longer positive in sign, but now point downward after the second injection point. This change from an endothermic to exothermic interaction suggests that a new interaction is occurring when more HPL15 is added. Realizing that the HPL15 is known to interact with itself, as seen in Figure 4.9, it appears that the first two peaks correspond to HPL15 adsorbing to the COO particles, and the following peaks corresponding to the addition of more HPL15 layers onto the particles. In other words, this raw data may suggest that multiple layers of HPL15 could be forming on the particle surface.

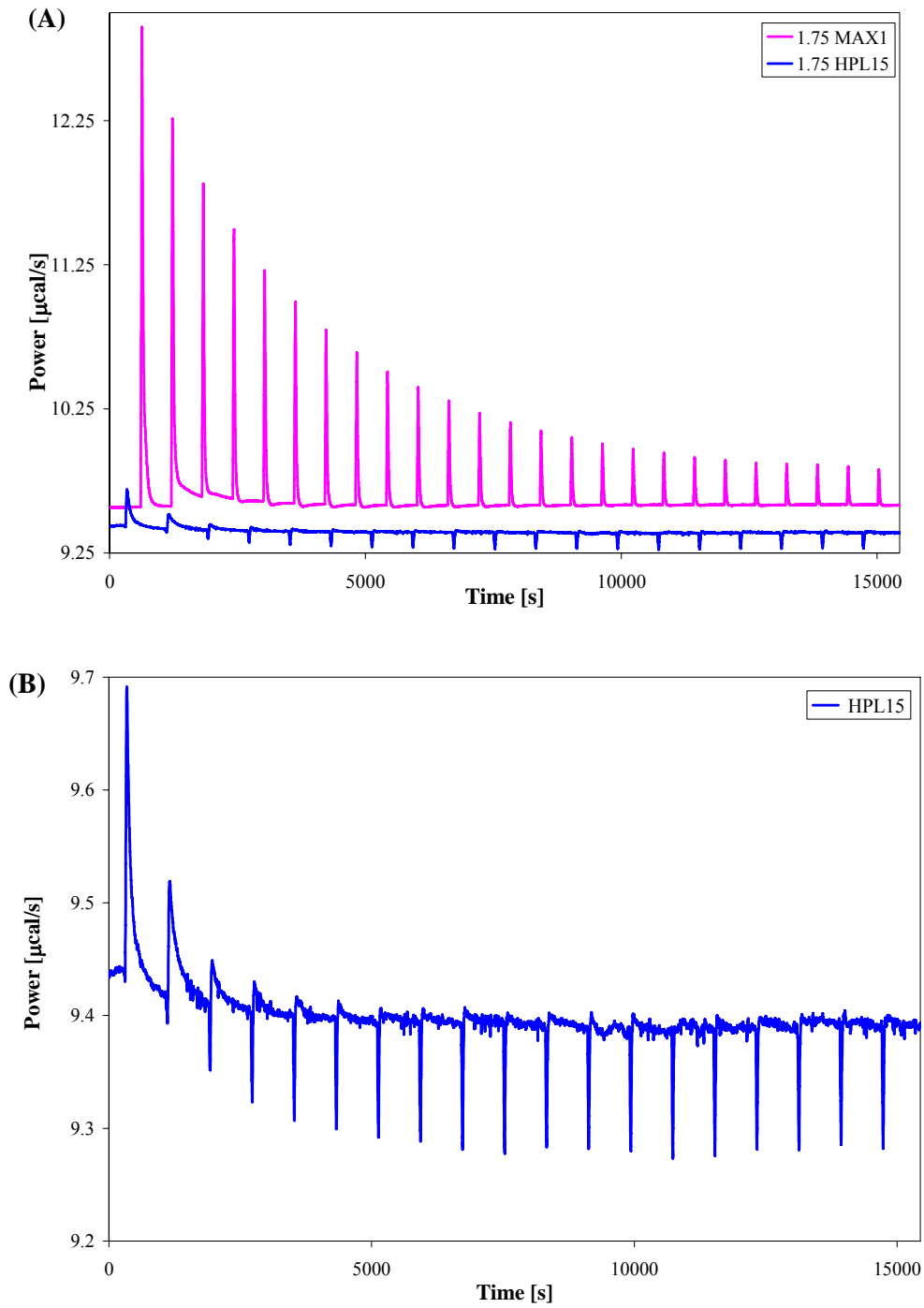


Figure 4.11. Measured signal for 0.175% MAX1 and HPL15 with COO. (A) Comparison between MAX1 and HPL15. (B) Magnified HPL15-COO data.

The final raw data curve analyzed was from the interactions between MAX1-NH₂ and HPL15-NH₂. Figure 4.12A shows this result, where the NH₂ interactions show similar trends to that of the Peptide-COO data. The MAX1-NH₂ peaks are significantly larger than the HPL15-NH₂ data (approximately 2 μ cal/s for the first two peaks). As seen in Figure 4.12B, the MAX1-NH₂ peaks become successively weaker initially as more peptide is being added to the solution as the binding sites are being occupied. The HPL15 data maintains upward peaks for the first four peaks, and there is no evident peak at the fifth point. Thereafter, the peaks increase magnitude in the negative direction until reaching a saturation point where the peaks maintain their magnitude. Similar to the HPL15-COO interactions, this result suggests that multiple layers are being added to the particle surface. The fact that four peaks point upwards for the NH₂ compared to only two for the COO raw data suggests that more peptide adsorbs to the surface of the NH₂ particles before the multiple peptide layers become prevalent.

As with the MAX1 raw data, the absorbed heat from each injection of the HPL15 corresponds to the area under each of these injection peaks. Thus, integration of these peaks yields the total heat per mole of injectant as a function of the peptide concentration. Figure 4.13 shows the result of this integration after subtracting both the peptide and particle blank titrations. As in the MAX1 analysis, the binding enthalpies of the HPL-particle interactions are found by extrapolating this integrated data to the theoretical heat

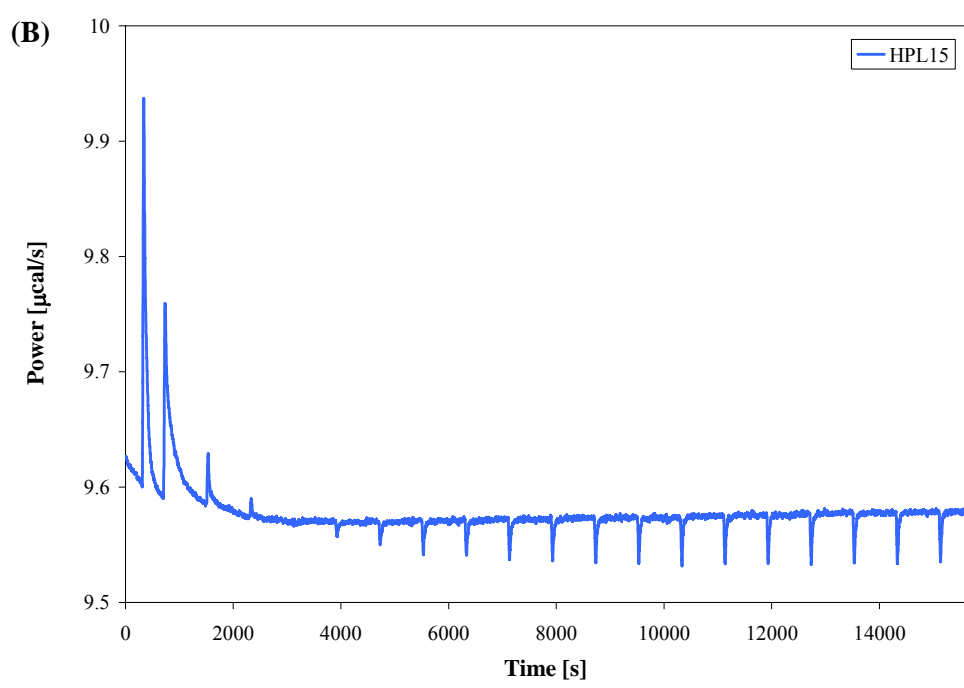
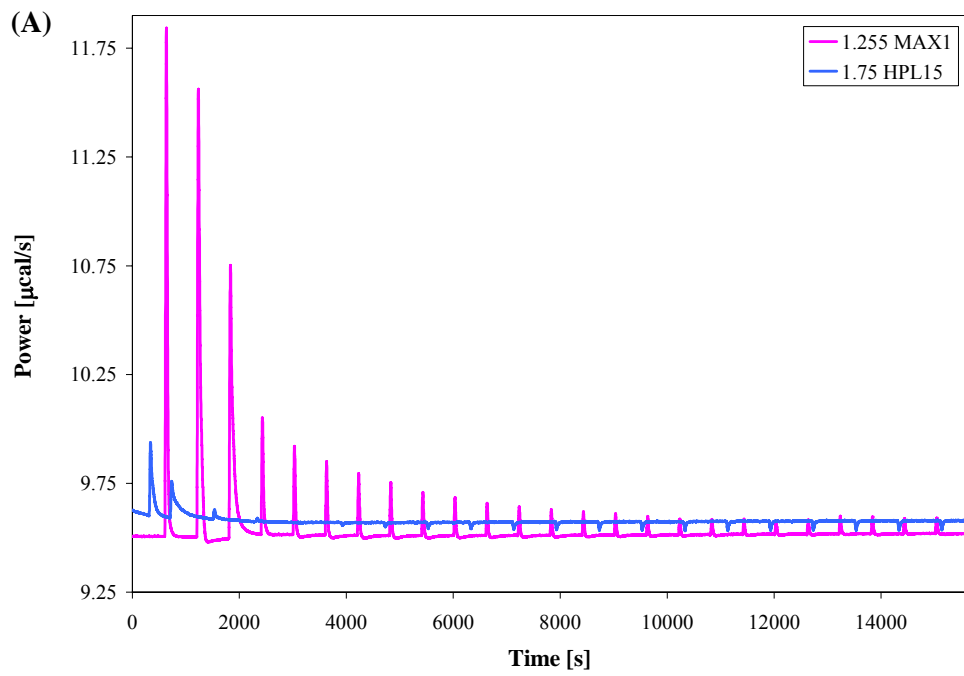


Figure 4.12. Measured for 0.126% MAX1 and 0.175% HPL15 with NH_2 . (A) Comparison between MAX1 and HPL15. (B) Magnified HPL15- NH_2 data.

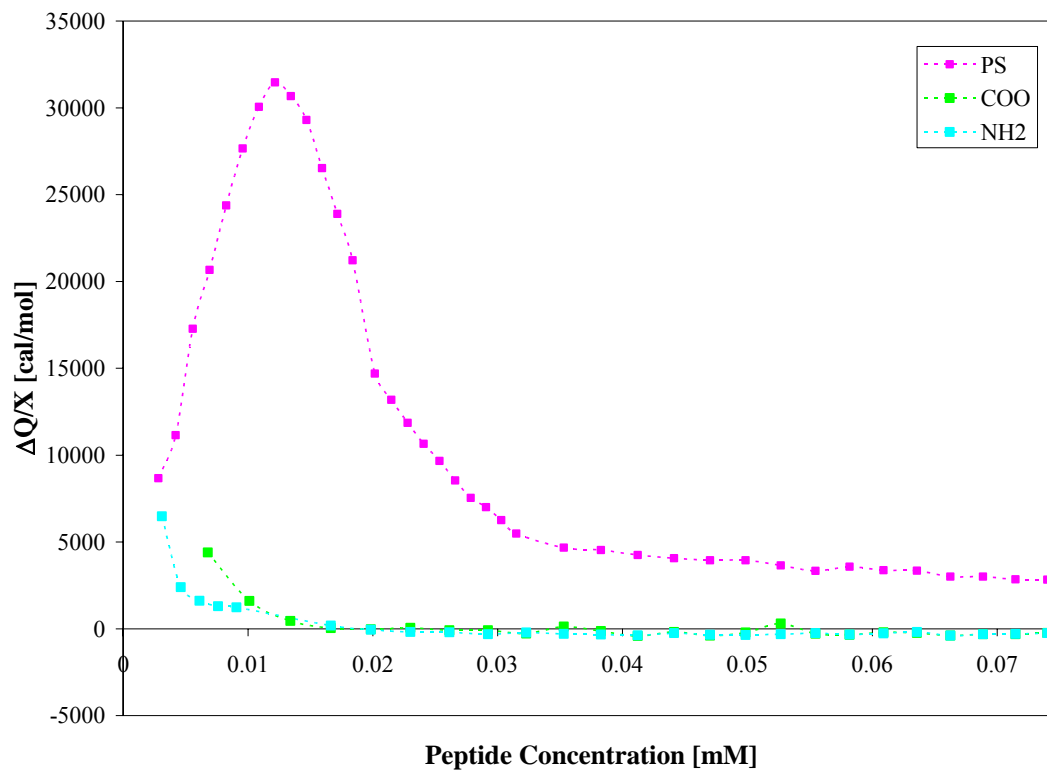


Figure 4.13. $\Delta Q/\Delta X$ results for 0.175% HPL15 with PS, COO, and NH₂.

Table 4.3. Binding enthalpies for HPL15-PS, COO, and NH₂.

	PS	COO	NH₂
[*] ΔH _f [kJ/mol]	14.2 +/- 2.3	86.6 +/- 6.2	44.6 +/- 12.5

^{} Assuming no heat from peptide-peptide interactions initially*

absorbed at zero peptide concentration. Table 4.3 shows the result of this extrapolation. Although there are most likely two binding enthalpies for HPL15: those with the particles and self interaction heats, it was assumed that the initial heat of binding calculated in the aforementioned way was mostly (if not entirely) from the interactions with the particles. This assumption seems logical because there is a much smaller degree of peptide for HPL15 to interact with than particles. With this assumption, a comparison of the binding enthalpies to the MAX1 results is shown in Figure 4.14. As expected, Figure 4.14 shows that the heats of binding for the MAX1 interactions are much stronger than for the HPL15 interactions. Figure 4.14 also reveals that the same trend is occurring between the particles in the two data sets despite the unique interactions observed in the HPL15 data.

Using the integrated data shown in Figure 4.13, in conjunction with Equation (4), we arrive at the total heat absorbed as a function of the peptide concentration. Figure 4.15 shows this result, where it indicates that the HPL15-PS interactions absorb significantly more heat than the COO and NH₂ interactions. As there are two sources of binding enthalpies for the HPL15 data, the total amount of absorbed heat could not be normalized from the heats of binding as was done with the MAX1 data. This is because the binding enthalpies have two contributions and the contributions may vary throughout the process.

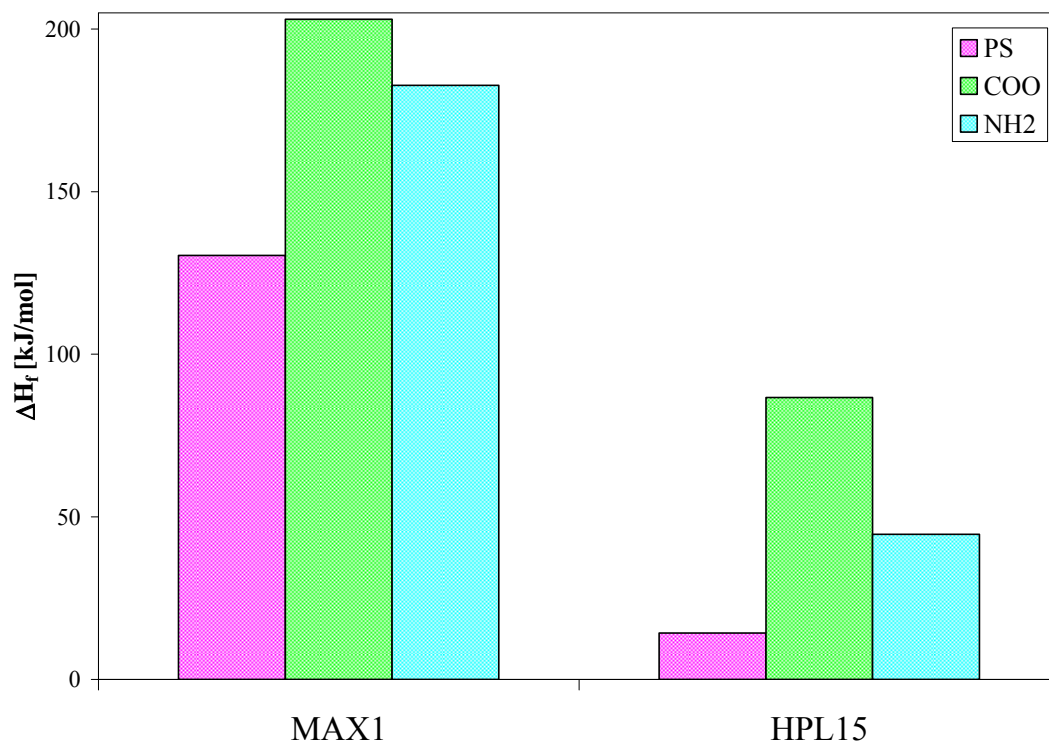


Figure 4.14. ΔH_f comparison between MAX1 and HPL15.

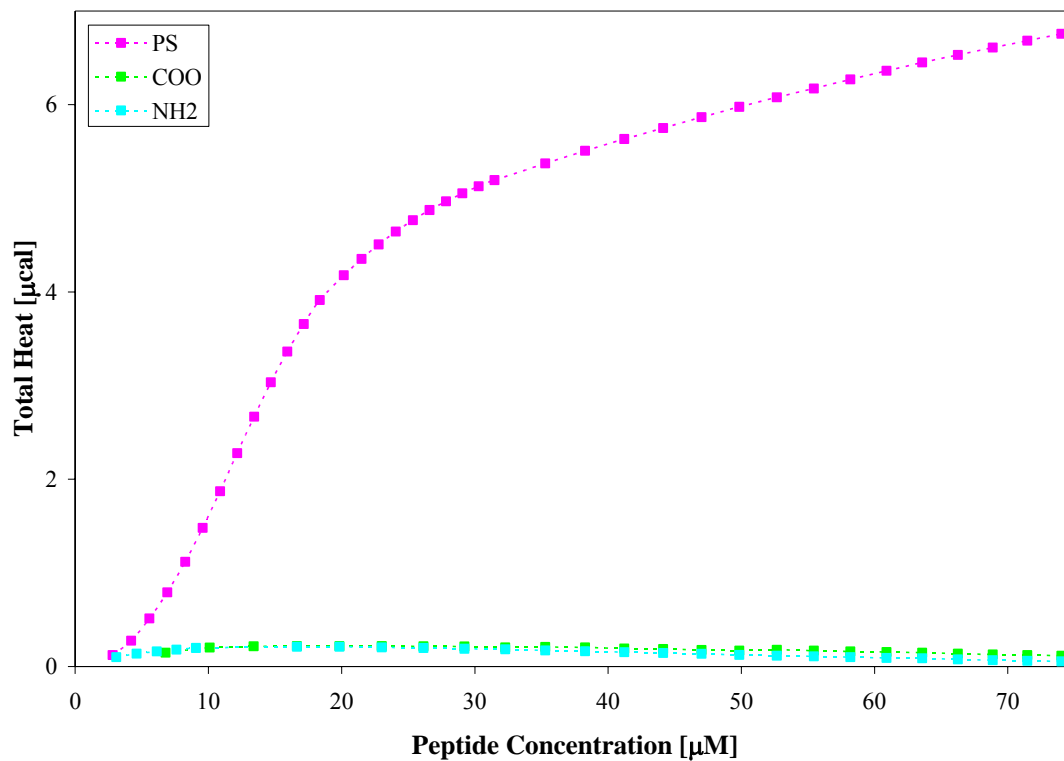


Figure 4.15. Total amount of absorbed heat for HPL15 with PS, COO, and NH₂. (Dashed lines just illustrative-no fits.)

While Langmuir fits could not be fit to any of the HPL15 data because they each suggest more complex mechanisms and the normalized heat results indicative of the degree of binding could not be determined, comparisons between the MAX1 and HPL15 total heat results are shown to better understand the complexity involved in each of the mechanisms.

Figure 4.16 shows the total heat comparisons between the MAX1 and HPL15 interactions with PS. This figure shows the simple curve for the MAX1-PS heat which is depictive of the Langmuir isotherm, where the curve begins to level off. Conversely, the HPL15-PS heat curve indicates a more complex mechanism, where there is an initial sigmoidal shape followed by a continual increase in heat absorbed. The absence of a plateau suggests the data may be better represented by multiple layer isotherms such as the Freundlich isotherm and the Brunauer-Emmet-Teller (BET) isotherm. Despite this similarity, there may be more complex isotherms which describe these interactions more accurately.

Because the HPL15-COO interactions change from an endothermic to an exothermic process, the total heat could be interpreted in terms of the total heat or the absolute values of the total heats. With this in mind, Figure 4.17A compares the MAX1-COO and HPL15-COO interactions for both total heat and absolute total heats. Figure 4.17A clearly indicates that the total heat from the interactions is significantly higher for the MAX1-COO interactions than the HPL15-COO interactions regardless of how the heats were attained. Figure 4.17B shows the HPL15-COO on a smaller scale where the shape of the curves can be more easily noted. Figure 4.17B shows that the net total heat

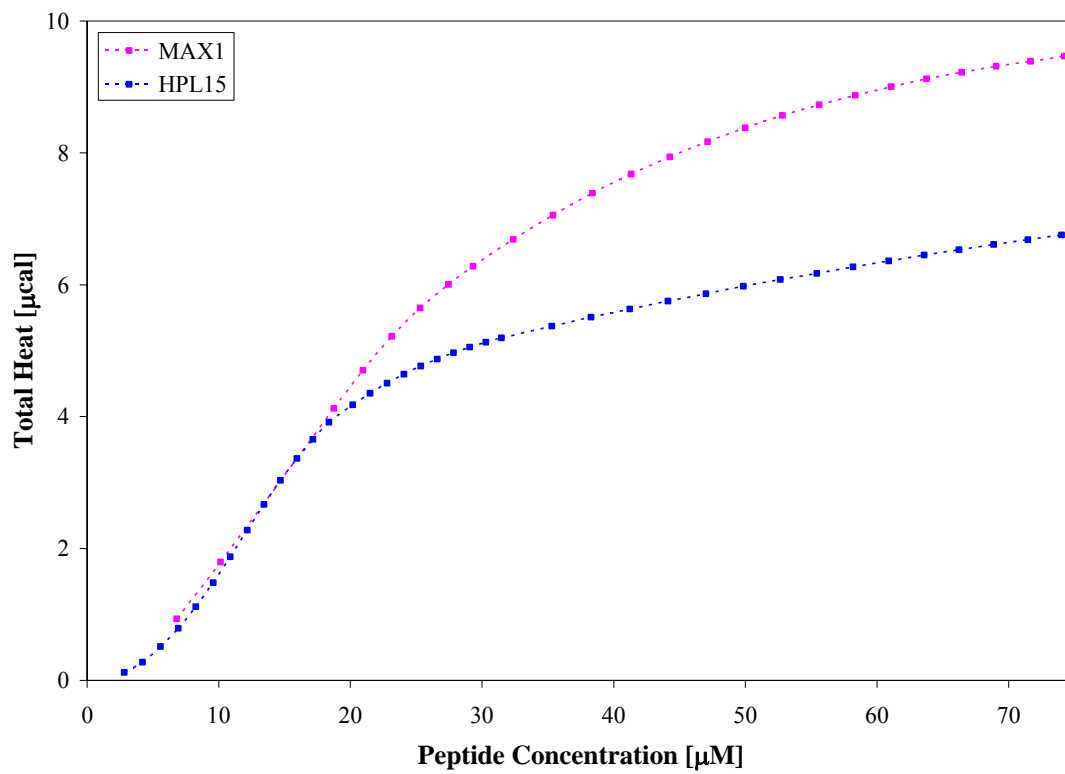


Figure 4.16. Total amount of absorbed heat for MAX1-PS and HPL15-PS.

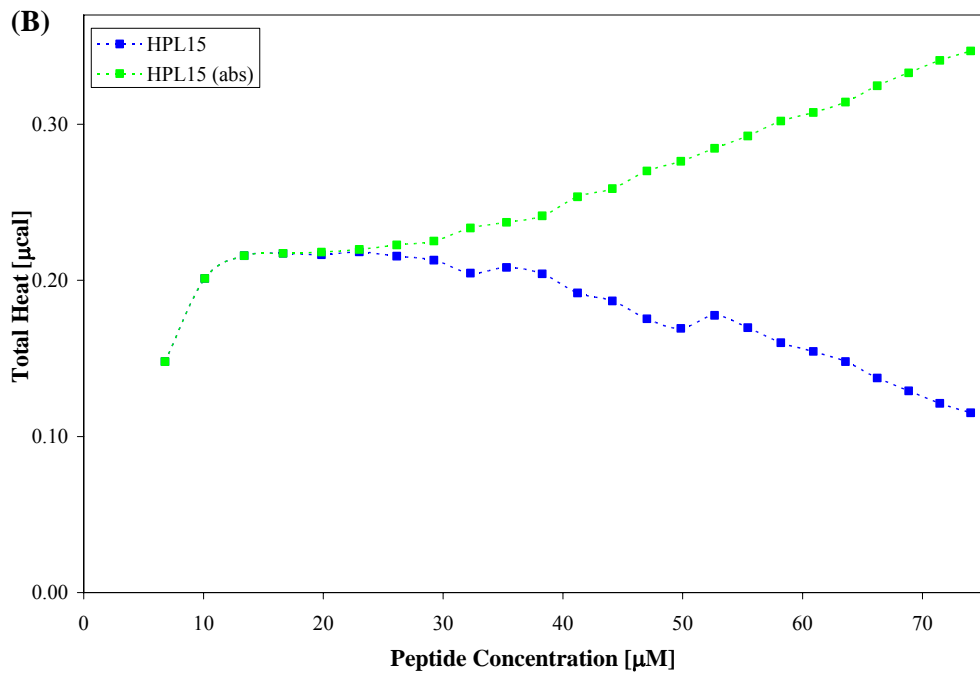
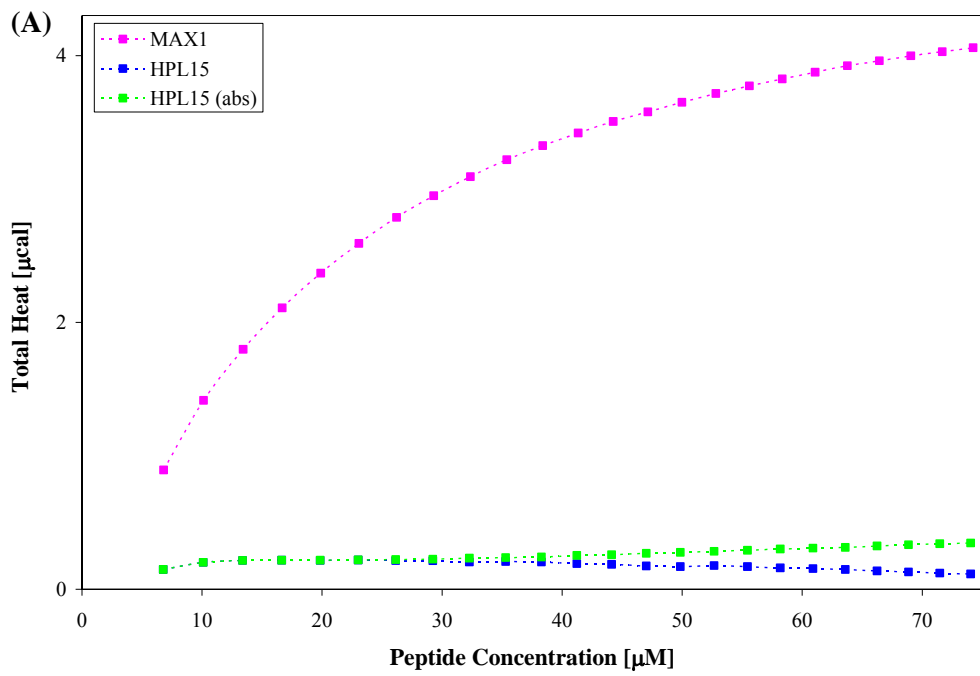


Figure 4.17 Total amount of absorbed heat for MAX1-COO and HPL15-COO. (A) Comparison between MAX1 and HPL15. (B) Magnified HPL15-COO data.

actually decreases over the course of the reaction. If the proposed mechanism is correct, the HPL15 initially adsorbs to the particle surface, and an endothermic process is primarily observed in the ITC. At higher peptide concentrations, HPL15 binds to itself, and an exothermic process is primarily observed in the ITC. These two processes could occur in two schematics, shown below.



The first scheme suggests that the HPL15 preferentially binds to the HPL15 that has already bound to the COO surface, whereas the second scheme suggests that the reactions are competing, where the HPL15 is likely to bind with itself regardless of whether the other HPL15 molecule is free or already bound to the COO surface. The absolute total heat curve in Figure 4.17 may support the former case, where the shape of the absolute heat curve is very similar to that of the Freundlich and BET isotherms, which account for multiple layers on the particle surfaces. However, further studies will be needed to assess the validity of either of these descriptions.

Figure 4.18A shows the total heat and absolute total heat for the MAX1-NH₂ and HPL15-NH₂ results. This figure shows a similar result as the MAX1-COO and HPL15-COO comparison. The MAX1-NH₂ interactions have a much stronger heat associated with it than the HPL15-NH₂ interactions, though these differences are less than for the COO data. Figure 4.18B shows a similar curve for the HPL15-NH₂ and HPL15-NH₂ (abs) data as the HPL15-COO data, suggesting that similar mechanisms are likely.

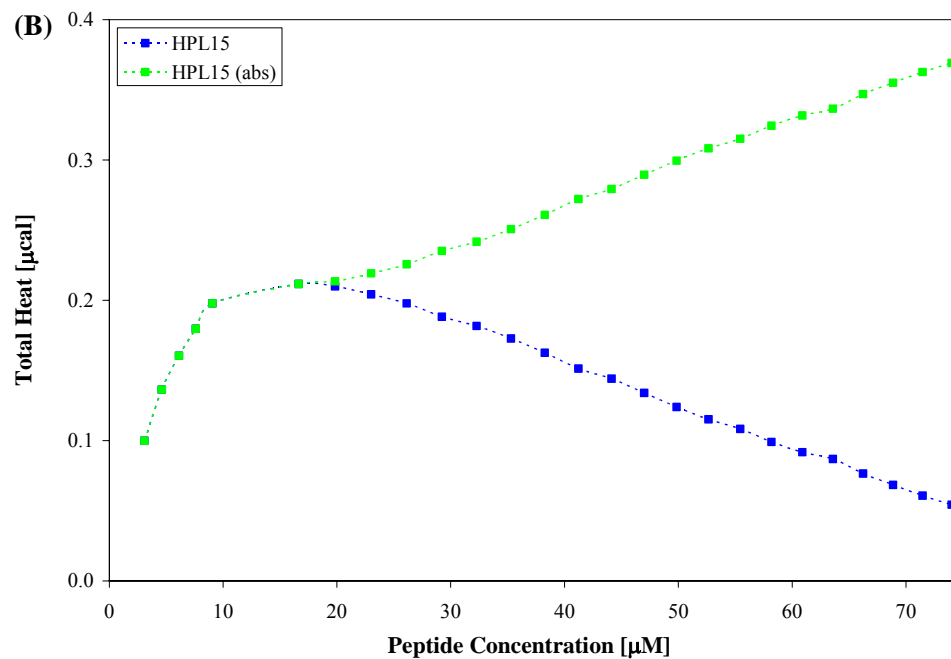
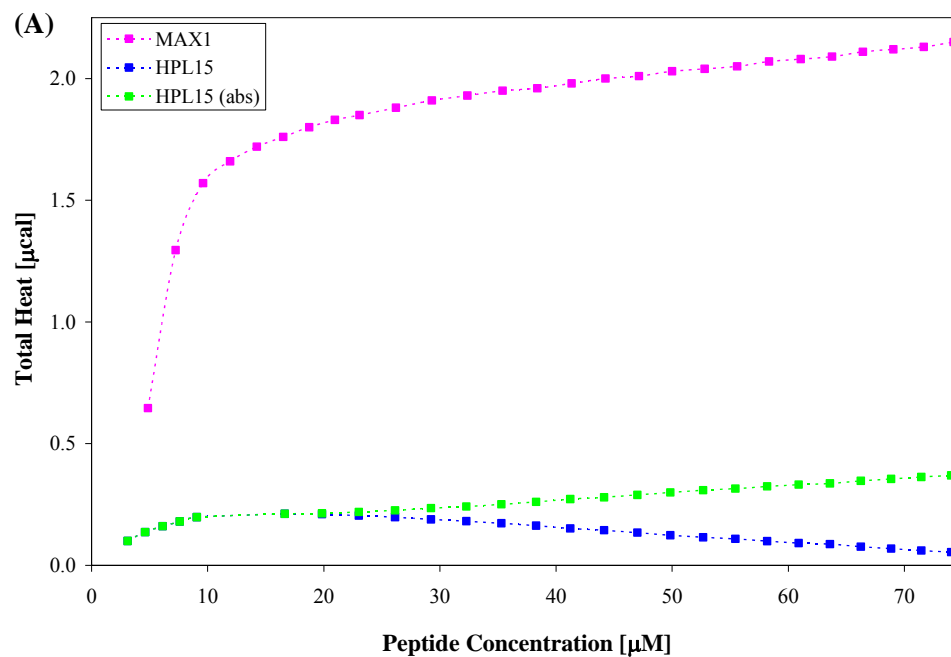


Figure 4.18. Total amount of absorbed heat for MAX1-NH₂ and HPL15-NH₂. (A) Comparison between MAX1 and HPL15. (B) Magnified HPL15-NH₂ data.

Although total number of binding sites could not be accurately found for the HPL15 results because the mechanisms involved are more complex than the Langmuir isotherm, the degree of peptide adsorption per surface area was approximated for both the MAX1 and HPL15 data. However, it should be noted that these results assume that the heat observed from the ITC experiments arises from the adsorption to the particle surface, or to the surface of peptide already on the particle. In other words, this approximate surface area coverage analyze is only valid if scheme 1 is accurate for the COO and NH₂ results. **Thus, this analysis needs more substantiated evidence of the HPL15 interactions to be validated.** Figure 4.19 shows these results, and indicates that more peptide adsorption occurs with MAX1 than HPL15 when interacting with the PS and COO particles. This suggests that HPL15 has fewer binding sites available to it on both the PS and COO particle surfaces. This result makes sense in that the HPL15 has a lower net negative charge, so that the peptide has fewer residues which will interact with the PS and COO surfaces. However, the NH₂ results suggest that there is more peptide adsorption occurring on the particle surfaces for the HPL15 than the MAX1 peptides. This result makes sense when noting the surface chemistry differences in the substituted residue. The PS and COO particles have less affinity to interact with the HPL15 than MAX1 because HPL15 carries a carbonyl group in addition to the amine group, which promotes stronger repulsive interactions with the PS and COO particles than only the amine group would. However, because the NH₂ particles have no oxygen in its terminal location, it has an equal repulsion to the glutamine residue as the lysine residue.

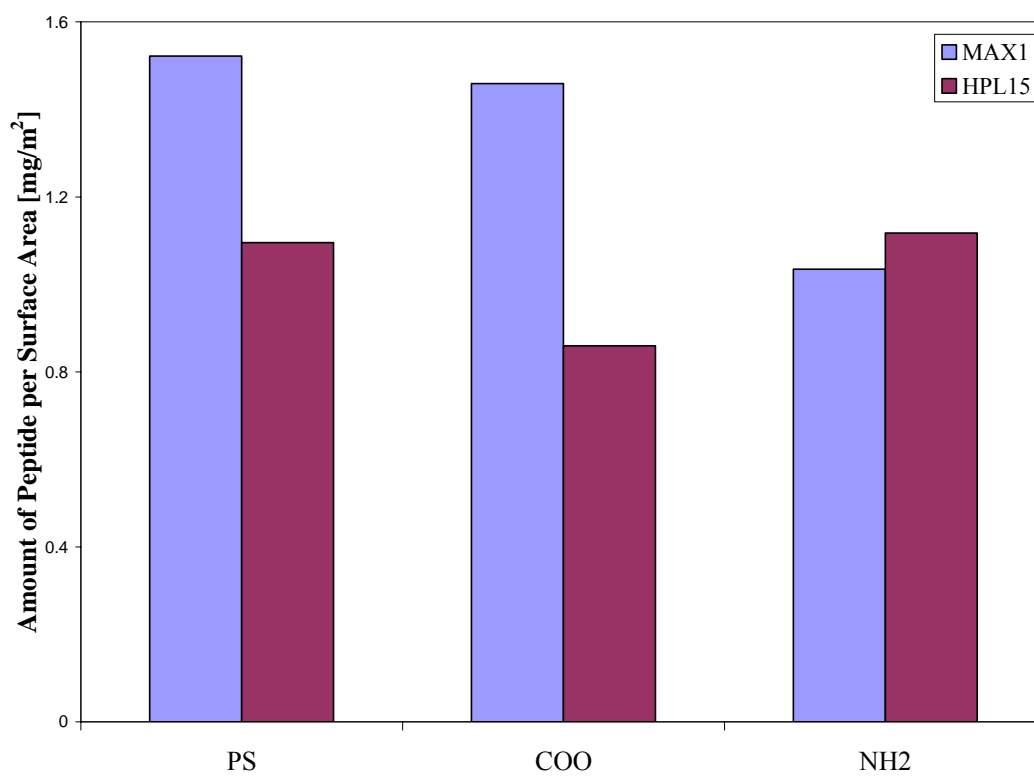


Figure 4.19. Comparison of the amount of peptide adsorption to PS, COO and NH₂ for MAX1 and HPL15.

Table 4.4. Material pHs(and pKas) in nanopure water.

	MAX1	HPL15	PS	HPL15 & PS	COO	NH ₂
pH	5.13	5.43	9.40	6.85	4.20	6.30
pKa	10.5	---	~2	---	~5	---
Proton affinity [kJ/mol]	---	---	1294.1 ²³	---	540.5 ²⁴	773.4 ²⁴
<i>*Particle pKa values from DukeScientific</i>						

4.3.3 pH Interactions in ITC

ITC experiments are traditionally conducted in buffered solutions to prevent interactions arising from changes in pH. However, no notable interactions were observed between HPL15 and any of the microsphere particles when experiments were conducted in 40nM NaAc pH 5 buffer (data not shown). The difficulty with characterizing interactions when in buffered systems lies in the fact that the cations present in the buffer systems interact with the solute ions which potentially suppresses interactions which would occur between the peptide and particles had their surface charges not been suppressed by the buffer solution. Because the purpose of this thesis was to capture the interactions occurring in typical microrheological measurements, which are often conducted with water solvents, this paper focused on experiments conducted in nanopure water solutions. With this in mind, it is important to recognize the native pH environments of each of the species to properly identify changes in pH when interpreting the experimental results. Table 4.4

²³ Dixon, D.A. Bronsted Basicities and Lewis Acidities. *University of Alabama*.
<http://72.14.207.104/search?q=cache:STOIQF04l0QJ:www.er.doe.gov/bes/chm/Publications/Contractors%2520Meetings/CatalysisContrMtg2004/catalysis%2520contractors%2520input/7%2520Theory/Dixon.ppt+Br%C3%B6nsted+Basicities+and+Acidities+and+Lewis+Acidities+for+WO+and+MoO+clusters&hl=en&gl=us&ct=clnk&cd=1&client=firefox-a>

²⁴ Hunter, E.P; Lias, S.G. *Journal of Physical Chemistry Reference Data* **1998**, 27, 3, 413-656.

indicates that pH differences are strongest between HPL15 and PS and weakest between HPL15 and NH₂. With nearly 4 unit differences between HPL15 and PS, pH could potentially play a strong role in the interactions involved in microrheological measurements if the HPL15 or PS pKa values were within these unit differences. However, the both pKa values fall outside these bounds. While the pKa of MAX1 is just over 1 pH unit above the PS solution, the addition of MAX1 consistently decreases the solution pH to below the MAX1 pKa. Thus, the only substantial concern may arise from COO particles because its pKa is less than 1 unit away from both peptide solutions. However, the proton affinities of each of the particle charge groups are orders of magnitude larger than those seen in these experiments. In this way, proton heats of ionization would have flooded the observed conditions had they been occurring in these experiments. Because this was not the case, it is doubtful that heats associated with protonation or deprotonation are a contributing factor in the aforementioned analysis.

Chapter 5

CONCLUSION

Microrheology uses the thermal motion of small particles embedded within a material to characterize the viscous and elastic properties of this complex fluid. Interactions between the embedded particles and the material are inevitable, and lead to changes in the local environment which results in potential systematic errors with every measurement. A quantitative assessment of these interactions allows a better understanding of the effects these interactions have on microrheological measurements. Thus, this thesis looked to quantitatively characterize the interactions occurring between two peptides, MAX1 and HPL15, and four particle types, PS, COO, NH₂, and PEG. This analysis was done using multiple particle tracking and isothermal titration calorimetry.

Multiple particle tracking of the gelation kinetics of MAX1 with variously sized PS and COO particles in a pH 9 borate buffer indicated surface chemistry interactions between MAX1 and these particles because the mean-squared displacements curves were not overlapping. This result indicated the breakdown of the generalized-stokes-einstein relationship and suggested peptide adsorption. Video microscopy images of MAX1 and PS, COO, NH₂, and PEG in pH9 borate buffer indicated that the hydrophobic PS and COO particles were mono-dispersed and stable within the MAX1 medium, while the NH₂ and PEG particles clustered in the presence of MAX1, indicating instability.

ITC was used to quantify the interactions occurring between both peptides and all four particle types. Water was used as the solvent in each of the ITC experiments to accurately portray many microrheological measurements, so changes in pHs were occurring when the peptides and particles were combined. However, analysis was conducted assuming the changes in pH did not strongly affect the heats. The MAX1 with particles experienced endothermic adsorption for all cases, where the PS particles had the most particle adsorption, followed by COO, and NH₂. However, PEG had unique interactions with MAX1 where it was hypothesized that the particles clustered in the presence of MAX1, which would account for the large initial peak in the $\Delta Q/\Delta X$ data. Langmuir fits of the PS, COO, and NH₂ data with MAX1 indicated that NH₂ had the strongest binding affinity for MAX1, followed by COO, and PS. Although this result may initially appear to contradict the fact that PS experienced the most peptide adsorption, the results make sense when realizing that PS had the most binding sites available for MAX1, while NH₂ had the fewest.

ITC experiments with HPL15 and PS, COO and NH₂ were then conducted. With only a single one point mutation of the 15th amino acid residue from lysine to glutamine, HPL15 had a very similar surface chemistry to that of MAX1. However, this subtle change had a drastic effect on the peptide-particle interactions occurring. All of the interactions suggested complex mechanisms which could not be described by the simple Langmuir Isotherm. Rather, the HPL15-PS data indicated a maximum saturation point, where below this point, peptide adsorption increased with concentration, and above which the peptide adsorption decreased with concentration. The mechanism involved

with this is inevitably complex, however the net reaction was endothermic throughout the course of the experiment. The HPL15-COO and HPL15-NH₂ had a far different result, where the initial interactions were endothermic, and then an exothermic interaction(s) was observed. Two potential schemes were proposed from this result, one of which suggested that the peptide initially bound to the particle surface in an endothermic reaction, and then the peptide bound to the peptide already on the particles, forming multiple layers. However, further investigation of all the HPL15-particle interactions is needed for a better understanding of the complex mechanisms involved.

All of the results shown here clearly indicate the importance in characterizing the interactions involved between any material being analyzed and the particles embedded within it. Multiple particle tracking experiments with MAX1 and variously sized PS and COO particles revealed that different mean-squared displacements were observed for the different conditions. This indicated that the interactions between the particles and MAX1 have an effect on the microrheological results being measured. Thus, characterization of these interactions is necessary in order to properly explain microrheological results, especially when considering that the microrheological analysis techniques require that no interactions are occurring. It was shown here that ITC could become an excellent method of characterizing these interactions, and can allow a better understanding of the potential mechanisms involved in these interactions. Although no set method of accounting for the potential systematic errors arising from material-particle interactions in microrheological measurements is derived from the ITC data, the experiments allowed a much better

understanding of the interactions involved and help one to see the potential errors occurring from their experiments.

Appendix A

PEPTIDE ADSORPTION CALCULATIONS

To find P_{sat} (amount of protein required to saturate 1 microsphere)

1. Find injection point that begins the equilibrium curve from the raw data figure (where the horizontal portion begins)
2. Determine the total amount (mg) of protein injected into the sample
 - a. Column W in “integrated_data” excel sheet
3. Determine the number of microspheres in the sample
4.
 - a. PS:

$$\begin{aligned}(\# \text{ of particles}) &= \frac{(6) \left(\text{particle concentration [g/mL]} \right) \left(10^{12} \left(\text{sample volume [mL]} \right) \right)}{\pi \left(\text{particle density [g/mL]} \right) \left(\text{diameter } [\mu\text{m}] \right)^3} \\ &= \frac{(6) \left(0.0265 \text{ [g/mL]} \right) \left(10^{12} \left(1.8 \text{ [mL]} \right) \right)}{\pi \left(1.05 \text{ [g/mL]} \right) \left(0.948 \text{ } [\mu\text{m}] \right)^3} \\ &= 1.01837 * 10^{11}\end{aligned}$$

- b. COO:

$$\begin{aligned}(\# \text{ of particles}) &= \frac{(6) \left(\text{particle concentration [g/mL]} \right) \left(10^{12} \left(\text{sample volume [mL]} \right) \right)}{\pi \left(\text{particle density [g/mL]} \right) \left(\text{diameter } [\mu\text{m}] \right)^3} \\ &= \frac{(6) \left(0.0265 \text{ [g/mL]} \right) \left(10^{12} \left(1.8 \text{ [mL]} \right) \right)}{\pi \left(1.05 \text{ [g/mL]} \right) \left(1.03 \text{ } [\mu\text{m}] \right)^3} \\ &= 7.93997 * 10^{10}\end{aligned}$$

$$(\# \text{ of particles}) = \left(\frac{\# \text{ of particles}}{\text{mL}} \right) (\text{sample volume [mL]})$$

c. PS-NH₂:

$$= (3.6 * 10^{10}) (1.8 \text{ [mL]})$$

$$= 6.48 * 10^{10}$$

$$(\# \text{ of particles}) = \left(\frac{\# \text{ of particles}}{\text{mL}} \right) (\text{sample volume [mL]})$$

d. PEG:

$$= (3.6 * 10^{10}) (1.8 \text{ [mL]})$$

$$= 6.48 * 10^{10}$$

5. Determine amount of protein on each microsphere

$$\left(\frac{\text{protein amount}}{\text{particle}} \text{ [mg / unit]} \right) = \frac{(\#2 \text{ value})}{(\#3 \text{ value})}$$

6. Determine protein mass per surface area

$$\left(\frac{\text{protein amount}}{\text{microsphere surface area}} \text{ [mg / } \mu\text{m}^2] \right) = \frac{(\#4 \text{ value})}{\pi (\text{diameter [}\mu\text{m]})^2}$$

Appendix B

LANGMUIR EQUATION DERIVATION

Assuming $[P] = P_T$:

Known Relationships

$$Q(P_T) = Q([P] + [P \cdot S]) = \Delta H([PS] - [P \cdot S]_0) = \Delta H[PS]$$

$$P_T = [P \cdot S] + [P]$$

$$S_T = [P \cdot S] + [S]$$

$$K_a = \frac{[P \cdot S]}{[P][S]} \quad \text{because } P + S \xrightleftharpoons{K_a} P \cdot S$$

Then, assuming $[P] = P_T$, we have

$$K_a = \frac{[P \cdot S]}{[P_T][S]} = \frac{[P \cdot S]}{[P_T](S_T - [P \cdot S])}$$

$$[P \cdot S] = \frac{K_a [P_T][S_T]}{1 + K_a [P_T]}$$

From this, we then have the final equation which was used in Origin to find K_a and S_T

$$\text{FINAL EQUATION: } Q(P_T) = \Delta H[P \cdot S] = \Delta H \left(\frac{K_a [P_T][S_T]}{1 + K_a [P_T]} \right)$$

Appendix C

SODIUM DODECYL SULFATE RESULTS

ITC experiments were conducted with sodium dodecyl sulfate (SDS) with PS. These results were interesting in that they clearly indicated the critical micelle concentration (CMC). The integrated data is shown below for 64.15 mM and 128.5 mM SDS.

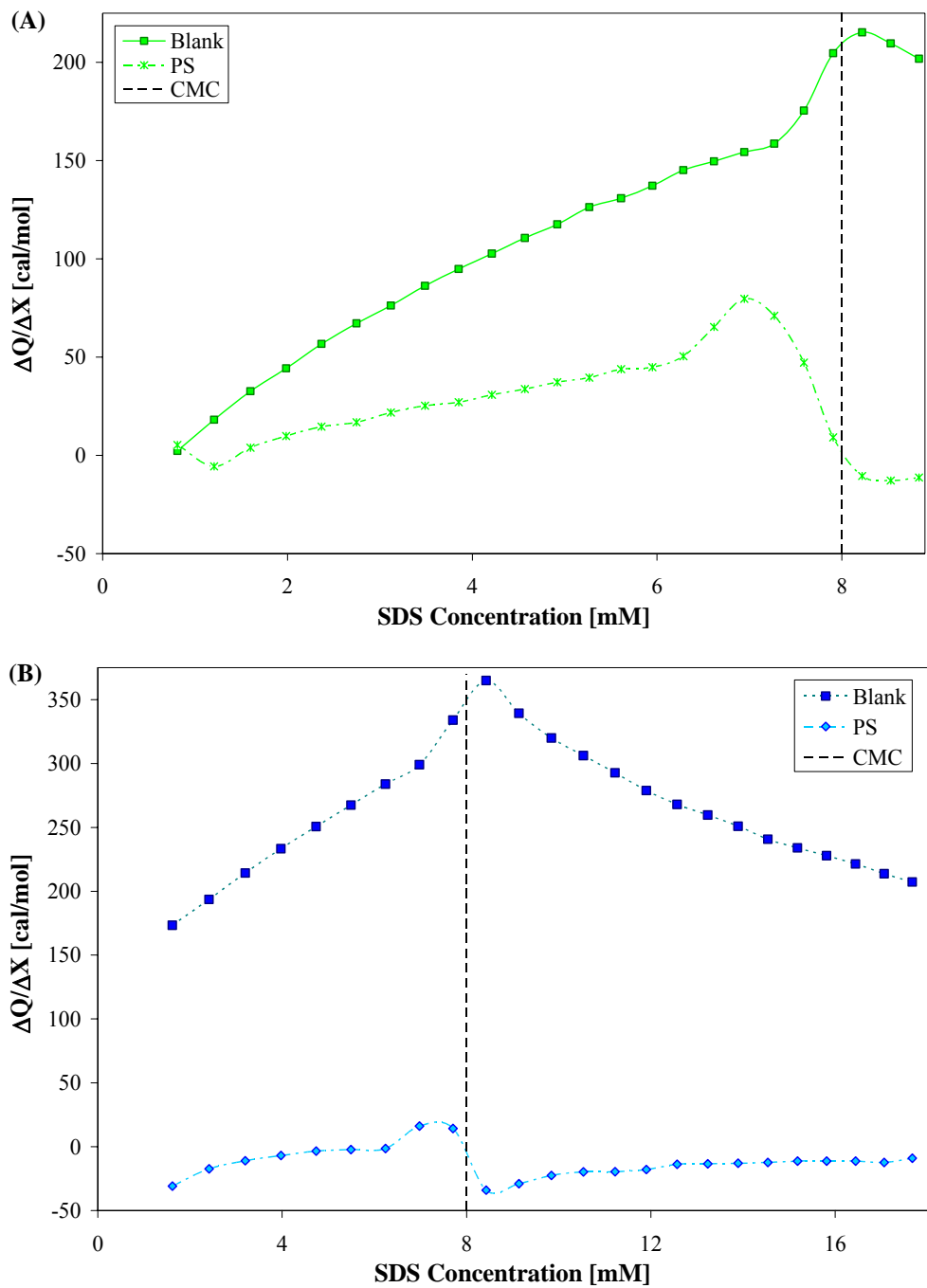


Figure A.1. $\Delta Q/\Delta X$ results for (A) 64.15 mM SDS and (B) 128.5 mM SDS titrated in water (blank) and with PS.

Appendix D

ACTIN RESULTS

ITC experiments were also conducted with Actin with PS and BSA coated PS. These experiments were conducted in buffer and the integrated data is shown below. As can be seen, there was no detectable interaction between actin and PS or BSA coated PS.

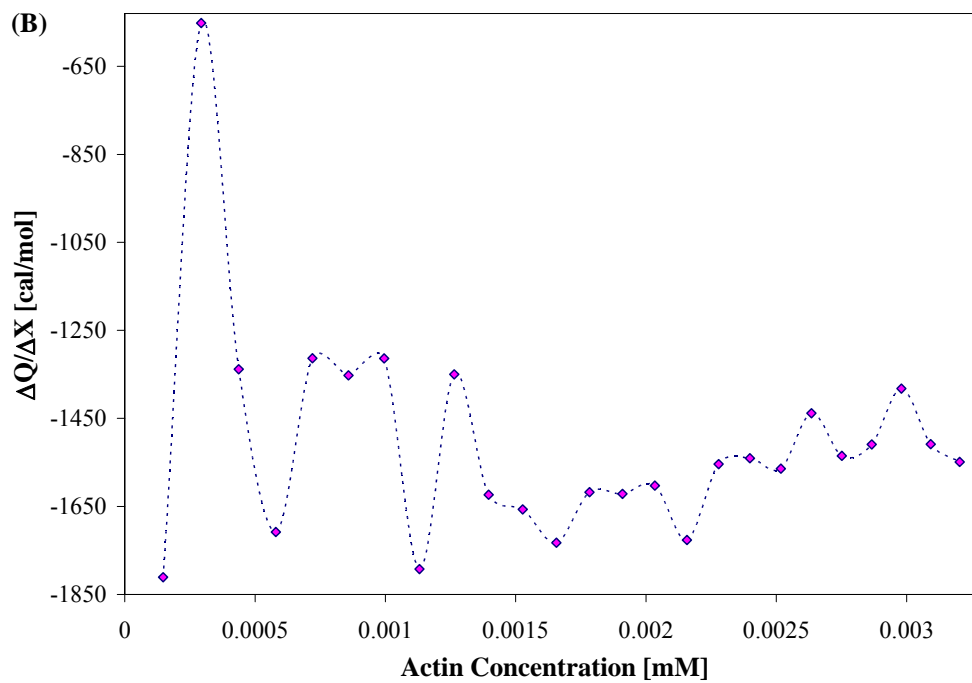
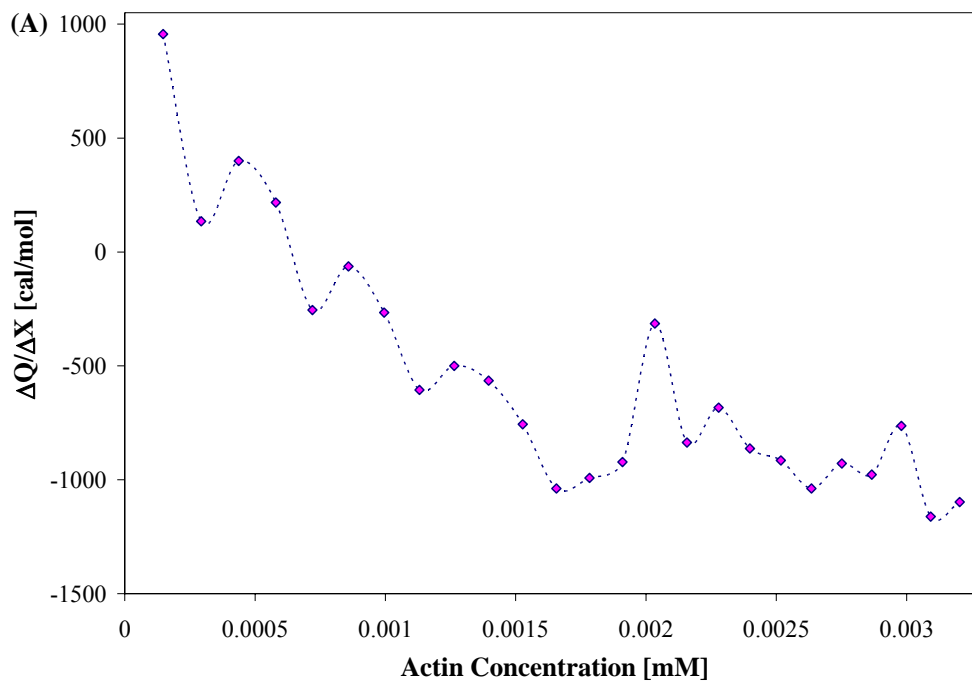


Figure A.1. $\Delta Q/\Delta X$ results for actin with (A) PS and (B) BSA coated PS.